Fuel 113 (2013) 873–897

Contents lists available at SciVerse ScienceDirect

Fuel

journal homepage: www.elsevier.com/locate/fuel

Parametric investigation of a renewable alternative for utilities adopting the co-firing lignite/biomass concept

N. Nikolopoulos [a,*], M. Agraniotis [a,b,1,2], I. Violidakis [a,1,3], E. Karampinis [a,c,1,4], A. Nikolopoulos [a,c,1,4], P. Grammelis [a,1,5], Ch. Papapavlou [d,6], S. Tzivenis [d,6], E. Kakaras [a,c,7]

[a] Centre for Research & Technology Hellas/Chemical Process and Energy Resources Institute (CERTH/CPERI), Greece
[b] Clean Energy Ltd., Athens, Greece
[c] Laboratory of Steam Boilers and Thermal Plants, Department of Mechanical Engineering, National Technical University of Athens, Athens, Greece
[d] Public Power Corporation S.A., Generation Division, Thermal Projects Engineering and Construction Department, Athens, Greece

HIGHLIGHTS

- CFD model for co-firing of biomass/lignite in a tangentially-fired pulverized-fuel boiler.
- Investigation of biomass size and its injection level on combustion efficiency and emissions.
- Vapor burners found to be the optimal injection point for biomass particles.
- Co-firing retrofit is highly profitable; dedicated biomass burners can also be considered.

GRAPHICAL ABSTRACT

(a) Induced velocity field and (b) NO_x concentration spatial distribution at burner levels for cases A.

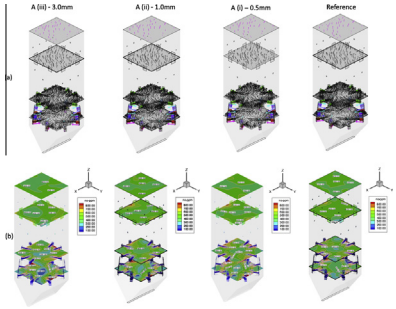

ARTICLE INFO

Article history:
Received 26 September 2012
Received in revised form 14 March 2013
Accepted 15 March 2013
Available online 10 April 2013

Keywords:
CFD
Co-firing
Lignite
Biomass
Economic evaluation

ABSTRACT

The purpose of the current paper is to investigate the *Cynara cardunculus* (cardoon)/lignite co-firing concept at a 10% biomass thermal share for a 330 MW_e pulverized fuel plant in Northern Greece. Two main cases are considered: (A) co-milling of pelletized biomass with lignite and (B) milling of balled and/or shredded material in dedicated biomass mills. A CFD model for plant simulation is developed taking into account the particularities of co-firing operation, in particular the non-spherical form of the biomass particle and its effect on the drag coefficient, devolatilization and combustion rates. Simulations are performed for the reference case of lignite-firing, which show good agreement with plant operational data, and for the two co-firing cases. Further subdivision of the co-firing cases is based on the biomass particle size and injection point in the furnace. In most co-firing cases, CFD results indicate that the substitution of lignite with biomass has minimal impact on the plant operational parameters as well as the potential for NO_x reductions. Increased unburnt losses in the fly and

* Corresponding author. Address: 4th km. N.R. Ptolemais-Kozani, 50200, Ptolemais, Greece. Tel.: +30 210 6501512; fax: +30 210 6501598.
E-mail addresses: n.nikolopoulos@certh.gr (N. Nikolopoulos), agraniotis@certh.gr (M. Agraniotis), violidakis@certh.gr (I. Violidakis), karampinis@certh.gr (E. Karampinis), a.nikolopoulos@certh.gr (A. Nikolopoulos), grammelis@certh.gr (P. Grammelis), c.papapavlou@dei.com.gr (Ch. Papapavlou), s.tzivenis@dei.com.gr (S. Tzivenis), ekak@central.ntua.gr (E. Kakaras).
[1] Address: 4th km. N.R. Ptolemais-Kozani, 50200, Ptolemais, Greece.
[2] Tel.: +30 213 0230100; fax: +30 210 6501598.
[3] Tel.: +30 213 0230101; fax: +30 210 6501598.
[4] Tel.: +30 210 6501509; fax: +30 210 6501598.
[5] Tel.: +30 210 6501593; fax: +30 210 6501598.
[6] Address: Aristotelous 30-32, 10433 Athens, Greece. Tel.: +30 210 8254065.
[7] Address: Heroon Polytechniou 9, 15780 Zografou Campus, Greece. Tel.: +30 210 7723604.

0016-2361/$ - see front matter
http://dx.doi.org/10.1016/j.fuel.2013.03.034

Nomenclature

A	pre-exponential factor in Arrhenius expression for char combustion, kg m^{-2} s^{-1} Pa^{-1}
A_{bio}	pre-exponential factor for devolatilization mechanism of biomass, s^{-1}
A_{lig}	pre-exponential factor for devolatilization mechanism of lignite, s^{-1}
A_p	heat transfer surface area of the particle, m^2
A_{sph}	surface area of the droplet, m^{-2}
Bi	Biot number, dimensionless
C	linear-anisotropic phase function coefficient, dimensionless
C_D	drag coefficient, dimensionless
CF_t	net cash flow of the investment within a period t
C_p	specific heat per unit mass, kJ kg^{-1} K^{-1}
D_0	mass diffusion limited rate on char burnout, kg m^{-2} s^{-1} Pa^{-1}
d_p	particle diameter, m
E	activation energy for char combustion, J kmol^{-1}
E_{bio}	activation energy for devolatilization mechanism of biomass, J kmol^{-1}
E_{lig}	activation energy for devolatilization mechanism of lignite, J kmol^{-1}
f_h	fraction of heat from char combustion absorbed by the particle, dimensionless
G	incident radiation, W m^{-2} sr^{-1}
g_i	gravitational acceleration for the i direction in Cartesian coordinates, m s^{-2}
h	convective heat transfer coefficient, W m^{-2} K^{-1}
h_{fg}	latent heat of vapourization, J/kg
H_{reac}	heat released by the char combustion reaction, J/kg
IRR	Internal Rate of Return, %
m_p	mass of the particle, kg
$M_{w,ox}$	molecular weight of oxides, kg kmol^{-1}
N	duration of investment, year
n	refractive index, dimensionless
n_{reac}	reaction order, dimensionless
Nu	Nusselt number, Nu = $h\ d_p/k_{oo}$
NPV	Net Present Value
Q_p	heat exchanged between the particle and the gas phase, J
r	discount rate, %
R	kinetic rate, kg m^{-2} s^{-1} Pa^{-1}
R_g	ideal gas constant, J kmol^{-1} K^{-1}
R_e	relative Reynolds number, dimensionless
t	time, s or year
T	gas temperature, K
T_p	particle temperature, K
TPC	Total Plant Cost
T_{oo}	temperature of the continuous phase, K
u_i	fluid phase velocity for the i direction in Cartesian coordinates, m s^{-1}
u_p	particle phase velocity, m s^{-1}
Y_{ox}	local mass fraction of oxidant in the gas

Greek letters

α	absorption coefficient, m^{-1}
ε_p	particle emissivity, dimensionless
Θ	shape factor, dimensionless
θ_R	radiation temperature, K
μ	molecular viscosity of the fluid, kg m^{-1} s^{-1}
ρ	fluid phase density, kg m^{-3}
ρ_p	density of particle, kg m^{-3}
σ	Stefan Boltzmann constant, 5.67×10^{-8} W m^{-2} K^{-4}
σ_s	scattering coefficient, m^{-1}
ϕ_{en}	enhancement factor, dimensionless

bottom ash can be expected when large biomass particles are combusted; the best scenario appears to be the separate milling of biomass and its injection in the vapour burners. Economic evaluation of the two cases also favours the dedicated milling system, despite its higher investment cost, due to the lower fuel cost of non-pelletized biomass. The co-firing concept appears to be highly profitable for the plant operator and further optimisation of the combustion process can be suggested by the installation of dedicated biomass burners.

1. Introduction

The improvement of the efficiency and the environmental performance, including reduction of greenhouse gas emissions, of fossil fuel utilisation for energy production has led to significant R&D efforts in the field of novel combustion technologies, such as oxy-fuel combustion [1] and flameless oxidation furnaces [2]. However, most of these technologies are in early stages of development and their implementation in existing fossil fuel power plants faces several limitations. Part of the solution in the quest for reducing GHG emissions from existing coal-fired power plants can be offered by biomass co-firing, a low cost technology option [3], the importance of which in reaching the EU targets for the increase of the share of renewable energy sources in the energy sector is well recognised by EU authorities [4] and research academy [5]. The most common technological option is direct combustion of the solid biofuels, although examples of syngas combustion after biomass gasification are also presented [6].

Co-firing is a particularly promising solution for GHG emissions decrease in Greece, due to the high installed capacity of lignite-fired power plants and the large contribution of indigenous lignite in the gross energy production [7]. However, instead of the usual, typically high quality biogenic feed stocks used in most of the co-firing power plants across Europe (saw dust or wood pellets), Greece will have to rely mostly on the locally produced agricultural biomass for reasons of decreasing the cost of the supply chain [8]. Despite the high availability of agricultural residues in Greece [9], the lack of mechanization for residue harvesting, the associated high operating costs and other competing uses have shifted attention towards the exploitation of locally grown energy crops for power generation. One of these crops to which Greek stakeholders have paid attention during the last years is *Cynara cardunculus* L. (cardoon), a perennial, herbaceous crop of Mediterranean origin well adapted to the xerothermic conditions of Southern Europe [10]. This is owed to its potential for high yields [11]. Cardoon is currently cultivated in the Region of Western Macedonia in the frame of a regional development program, aiming to produce biomass for combustion reasons for the nearby Kardia power plant [12].

An overview of co-firing experiences have been collected in review papers by [13,14]. Several studies concerning the modelling

of co-firing solid biomass along with coal in pilot reactors or large-scale pulverized boilers have been published [15–21]. A key factor outlined in most of the simulations is the large length to diameter ratio of biomass particles, which influences their trajectories inside the boiler and consequently their residence time and final burnout [16]. The co-firing of cardoon with a hard coal blend was investigated by [19] for a front-fired industrial furnace with an output of 350 MW_e, showing that is a promising fuel.

The purpose of the present study is to evaluate the effect of co-firing cardoon with Greek lignite in a 330 MW_e super-critical, Benson type, tangentially fired boiler, taking into account the major physical and chemical differences in the combustion process for cardoon and lignite. The optimal firing scheme is the main topic investigated in this paper, intending to add value to the investigations related to cardoon specifically or to biomass as an alternative fuel in general. The main parameters to be investigated are related to fuel burnout, temperature, gas species and NO_x spatial distributions for different firing concepts. The numerical results are evaluated on the basis of the aforementioned values at the furnace exit, within the furnace and at the hopper outlet. Numerical modelling of tangentially fired boilers have been performed by several authors [22–27], including studies on furnaces operating with low quality coals [28–30]. However, co-firing studies with lignite on tangentially-fired boilers have been limited to solid-recovered fuels [31].

In addition, an economic evaluation of the investigated co-firing is performed by taking into account all relevant project costs (Capital Expenditure – CAPEX, Operational Expenditure – OPEX) and calculating the main economic indices (Net Present Value – NPV, Internal Rate of Return – IRR, payback) for different cost cases of biomass and Green House Gas emission allowances. Combined, the two approaches offer an overall techno-economic optimisation of the biomass feeding and firing system for the investigated power plant.

2. Methodology

Following the approach presented in the Introduction, the methodology section is divided into two sections. In the first part, the methodology for the technical evaluation, i.e. the numerical simulations of the industrial boiler (CFD), is presented. More specifically, the basic numerical models applied in the CFD code are presented and the specific models developed for modelling the combustion behaviour of biomass particles are thoroughly described. In the second section, the methodology for the economic evaluation is presented.

2.1. CFD methodology

2.1.1. Basic numerical models

The computational domain includes the main combustion zone of the furnace; it excludes the convective part of the boiler. The implemented numerical mesh is built using the GAMBIT software and consists of 940.315 unstructured tetrahedral cells. The grid is locally refined in the near-burner area, the hopper region and the flue gas suction ducts in order to increase the accuracy of the numerical results near the boundary walls, since the heat flux transferred to the walls is a crucial parameter for the evaluation of the boiler operation. The grid density is comparable with the meshes employed in similar simulations of full-scale boilers [1,19,24,32,33]. This grid density has as also been validated as dense enough by performing simulations with a coarser numerical grid of around 700.000 cells; the deviations in the calculated flue gas characteristics at the furnace outlet are around 0.35% compared to the ones presented in this work. The smallest cell volume is equal to 4.42E−05 m^3 and the largest one equal to 0.268 m^3.

The numerical simulations are performed using the commercial CFD code Fluent v.12.1, [34] in a Pentium 4 2.4 GHz personal computer. Each run requires about 3 days of real computing time with parallel processing (4-CPU cores), including the NO_x simulations. The standard time averaged mathematical expressions of equations for mass, momentum, enthalpy and species are solved using the SIMPLE algorithm for predicting the flow, temperature and concentration of gas species within the boiler. All variables (velocity components, temperature, and gas species including NO_x) are solved using a second order Upwind scheme. The standard k–e model is used along with standard wall functions for the flow characteristics near the boundary conditions of boiler's wall.

Normally, the values of wall emissivity and wall temperature exhibit a spatial as well as a temporal distribution because of the different deposition rates of ash particles onto the heat exchangers. For a more valid simulation of the phenomenon, one should measure these rates either by pyrometers or thermal imaging cameras and use the extrapolated data as an input in the numerical model. In the present study, due to the lack of such data for this large scale industrial boiler, standard values are adopted. The wall temperature is set to a temperature equal to 365 °C, i.e. 50° higher than the average steam temperature in the steam tubes [19], whilst a typical value of 0.7 for wall emissivity is used [1,25,30,35–38]. The wall emissivity value is found to produce accurate results of the wall heat flux and furnace exit temperature for the reference case of lignite combustion.

The P1 radiation model for the simulation of the radiation heat transfer is used and the absorption coefficients of the gas phase are calculated using the domain based weighted-sum-of-grey-gases model (WSGGM), [34]. The transport equation for the incident radiation is given below:

$$\nabla \cdot (\Gamma \nabla G) - \alpha \cdot G + 4 \cdot a \cdot n^2 \cdot \sigma \cdot T^4 = 0, \quad (1)$$

where the parameter Γ is given by the equation:

$$\Gamma = \frac{1}{(3 \cdot (a + \sigma_s) - C \cdot \sigma_s)} \quad (2)$$

The impact of the discrete phase particles with the radiation model has not been considered in Eq. (1) in this work. The effect of the lignite particles on the radiation model is expected to be negligible, since both the particle emissivity and the convective heat transfer coefficient experienced by the particles are quite high: 0.9 and around 4500 W/m^2 K respectively. As a result, the temperature of the lignite particles is expected to be close to that of the surrounding gas. The larger biomass particles have a potentially larger impact on the incident radiation transport equation; therefore, these terms should be considered in future works, especially for higher biomass thermal shares or dedicated biomass combustion. In the present study however, the deviation is minimal due to the low share of biomass particles in the overall particle load of the boiler.

The furnace exit and the flue gas recirculation ducts are modelled using outflow boundary conditions. The relative distribution of flue gases between the recirculation ducts and the furnace exit is based on the heat and mass balance calculations for the milling system. Typically, 16.6–17.6% of the flue gas leaves the furnace through the flue gas recirculation ducts.

An Eulerian–Lagrangian description is adopted to resolve the coupling of gas with the particulate phase. The equations for the description of the two discrete phases (lignite and cardoon particles) are described in detail in the following paragraphs. Homogeneous gas phase reactions between species released during fuel devolatilization are modelled using the Finite Rate/Eddy Dissipation concept. Radiation and chemistry are updated every one (1) gas flow iteration. In the frame of this work, the reactions and

the corresponding Arrhenius rate coefficients used, are based on a Westbrook and Dryer 2-step global combustion mechanism for hydrocarbon fuels [16,20,39]. The mechanism is applied to two "artificial" species, LV and BV, representing the lignite and biomass volatiles respectively. Table 1 summarises the relevant reactions and associated rates.

2.1.2. Discrete phase modelling

Fuel particles are simulated in a Lagrangian fashion and particle trajectories are calculated throughout the whole computational domain. Particle dispersion by the induced turbulence of the gas phase is simulated using the stochastic tracking model, which includes the effect of instantaneous turbulent velocity fluctuations of the gas on the particle trajectories. The flow/particle interactions are represented by appropriate sink/source terms both in the gas/particulate equations, while these terms are updated once every 25 iterations of the gas fluid flow.

In co-firing simulations, the different behaviour of lignite and biomass particles deserves special attention. In the CFD simulations coal and lignite particles are considered as spherical and the equations of motion and combustion modes they obey can be handled by the pre-built models of most of the commercial CFD packages. On the other hand, biomass particles are highly irregular, and their approximation as spherical increases the deviation from real conditions. To reduce this deviation, in most cases they can be regarded as having a cylindrical shape. Thus, this affects both the induced drag force by the gas phase, while also increasing the heating, devolatilization and combustion rates. A parameter depicting the irregularity of solid particles is the shape factor Θ, which is the particle surface area of a sphere having the same volume as the particle divided by the actual surface area of the particle. For spherical lignite particles, it is obvious that Θ is equal to 1, while for biomass particles a constant value of Θ equal to 0.78 is used in the present study. This value is derived for a cylindrical shaped biomass particle, which length to diameter ratio is equal to 4. The value of 4 is a quite often value found in the literature and stands also for the investigated cardoon particles [16,19].

The particle equation of motion is solved for each trajectory. In order to ensure good statistics, a total of 102,050 particle-trajectories are simulated. The equation of motion for each particle is:

$$\rho_p \cdot \frac{du_p}{dt} = \frac{18\mu}{d_p^2} \cdot \frac{C_D \mathrm{Re}_p}{24} \cdot (u_i - u_p) + g_i \cdot (\rho - \rho_p) \quad (3)$$

For lignite particles, the drag coefficient is given by the standard equation of [40], while for biomass particles, the effect of non-sphericity on the drag coefficient is modelled using the equations of [41], which is the default Fluent model for non-spherical particles.

The fuel particles undergo five sequential heterogeneous steps: inert heating till the particle reaches the vapourization temperature; drying; inert heating till the particle reaches the devolatilization temperature; devolatilization; char burnout and a final inert heat step for the remaining ash particle. The calculations of the devolatilization and combustion rates of lignite and biomass particles can be performed by several sophisticated models, such as the Intrinsic Model, which take into account the chemical, molecular structure and the intrinsic surface of solid fuels. For this work, the chemical rate is calculated based on simpler Arrhenius models, due to restrictions on the availability of data for the investigated fuels.

Table 1
Kinetic rates for gas phase reactions.

Reaction	A $[s^{-1} \cdot n_{reac}^{-1}]$[a]	E (J/kmol)	Reaction order[b]
Westbrook and Dryer 2-step global combustion mechanism for hydrocarbon fuels			
$LV + O_2 \rightarrow CO + H_2O + SO_2 + N_2$	2.119×10^{11}	2.027×10^8	$[LV]^{0.2} \cdot [O_2]^{1.3}$
$BV + O_2 \rightarrow CO + H_2O + SO_2 + N_2$	2.119×10^{11}	2.027×10^8	$[BV]^{0.2} \cdot [O_2]^{1.3}$
$CO + 0.5\ O_2 \rightarrow CO$	2.239×10^{12}	1.702×10^8	$[CO] \cdot [O_2]^{0.25} \cdot [H_2O]^{0.5}$

LV: lignite volatiles, BV: biomass volatiles.
[a] n_{reac}: Total reaction order.
[b] Concentration values in (kmol/m^3).

For the devolatilization mechanism, a single rate model expressed in an Arrhenius form is adopted. For lignite, the pre-exponential factor is equal to $A_{lig} = 5 \times 10^{13}$ (s^{-1}) and the activation energy equal to $E_{lig} = 7.4 \times 10^7$ (J/kmol) [42]. For biomass, the corresponding rates are $A_{bio} = 9 \times 10^{18}$ (s^{-1}) and $E_{bio} = (2.39 \times 10^8$ J/kmol) [19].

Char combustion is modelled using a kinetic/diffusion limited model. Specifically for the Greek lignite particles the char combustion model and the kinetic parameters for two independent parallel reactions are described by Vamvuka et al. [43]. This model has also been implemented in the numerical model by using custom built functions, so as the results are more representative for the Greek lignite particles. For biomass combustion, the kinetics of the char combustion are modelled using a single step reaction the controlling parameters being equal to $A = 0.3272$ (kg/(m^2 s Pa)) and $E = 4.5758 \times 10^7$ (J/kmol) [19]. The overall biomass combustion rate, based on the kinetics/diffusion limited model is given by the following modified equation [34], where the standard expression is multiplied by the factor ϕ_{en}:

$$\frac{dm_p}{dt} = -A_{sph} \cdot \frac{\rho \cdot R_g \cdot T_\infty \cdot Y_{ox}}{M_{w,ox}} \cdot \frac{D_o \cdot R}{D_o + R} \cdot \phi_{en} \quad (4)$$

The burning enhancement factor, ϕ_{en}, was developed by Gera et al. [16] in order to take into account the fact that there is an increase in the overall burning rate of a cylindrical biomass particle compared to a spherical one of the same surface. The enhancement factor is given by the following simple algebraic function:

$$\phi_{en} = \frac{0.3 \cdot \Theta + 0.7}{\Theta} \quad (5)$$

The particle temperature T_p is calculated by considering the heat transfer due to convection and radiation, as well as the heat exchange with the surrounding gas during each step (drying, devolatilization, char combustion) using the following equation:

$$m_p \frac{d(C_p \cdot T_p)}{dt} = A_p \cdot h \cdot (T_\infty - T_p) + A_p \cdot \varepsilon_p \cdot \sigma \cdot (\theta_R^4 - T_p^4) + Q_p \quad (6)$$

The term Q_p in Eq. (4) refers to the heat exchanged between the particle and the gas phase through water vapourization, Eq. (5), or through the heterogeneous char combustion, Eq. (6):

$$Q_p = \frac{dm_p}{dt} \cdot h_{fg} \quad (7)$$

$$Q_p = -f_h \cdot \frac{dm_p}{dt} \cdot H_{reac}, \quad (8)$$

where h_{fg} is the latent heat of vapourization, H_{reac} is the heat released by char combustion and f_h is the heat fraction observed by the particle. In this work, the char burnout product is assumed to be CO_2 and the f_h is set to 0.3 [34,44].

It should be noted that the effect of non-sphericity for the biomass particles is taken into account in Eq. (6) by using the actual surface area of the particle and not that of the spherical equivalent. Moreover, for the cylindrical particles, the heat transfer coefficient is evaluated using the well suited for this case Churchill and Bernstein expression for the Nusselt number [45]. Intra-particle conduction of heat and mass are not considered in the present study. For the lignite, the calculation of the Biot number (=$h\ D_{eq}$/

k) yields values of 1.06, 1.51 and 1.48 for particles diameters of 50 μm, 90 μm and 170 μm respectively. Normally, for such values conduction within the particle volume is a limited factor, but according to [46–50] the heat transfer is limited by the internal conduction when Biot number is larger than 10. Therefore, for the lignite particles the neglect of heat conduction mechanism within the particle is not a coarse approach, but for the case of biomass particles this effect should be considered, as in the approach of [46], especially for cases when the biomass thermal share in the fuel mixture is high.

The char combustion model employed is based on the work of Smith [50], which assumes that oxygen fully penetrates the pores of the particles so that the particle diameter remains constant and the density is decreasing during combustion.

Due to limitations of the standard sub-models of the ANSYS/Fluent code, all steps one biomass particle undergoes during its combustion are implemented in the ANSYS /Fluent standard platform by the use of custom built User Defined Functions (UDFs).

To ensure the solution convergence the dimensionless residuals for the continuity equation should be less than 10^{-4}, while for the momentum, energy and NO_x calculations residuals should be less than 10^{-6} after the introduction of all submodels. Moreover, the area weighted averaged values of the main flue gas species concentrations and temperature at three representative horizontal levels of the boiler was monitored; if their values remains constant with less than 0.3% variation, then the solution is assumed to have reached convergence.

2.1.3. NO_x formation modelling

In the present study, both thermal and fuel NO_x mechanisms are considered. Prompt NO_x formation is not taken into consideration, since it is only relevant in fuel-rich conditions, uncharacteristic of pulverized fuel systems.

For thermal NO_x formation the extended Zeldovich mechanism is used. The mass transport equation for the NO, HCN and NH_3 species including their convection, diffusion, production and consumption mechanisms are solved. The transport equation for NO is solved by estimating the local concentrations of O and OH radicals through the partial equilibrium approach and taking into account the effect of turbulence interaction by the probability density function (PDF) [34].

Regarding the fuel NO_x mechanism, nitrogen oxides are produced by the oxidation of the nitrogen bound in the coal, both in the volatile matter and in the char. The HCN and NH_3 generally react with O_2 to form either NO in fuel-lean regions or with NO to form N_2 in fuel-rich regions [51].

Fuel bound N for the two examined fuels (lignite and cardoon) is considered to be distributed between volatiles and char at a ratio equal to the respective ratio of volatile and char content of the fuel. The nitrogen containing species released from volatiles are HCN and NH_3, with a ratio of 9:1 for lignite [52] and 1:9 for biomass [53]. Char bound nitrogen is considered to directly convert to NO, mainly as a desorption product from oxidised char nitrogen atoms [54]. A conversion factor of 0.7 is adopted for the char bound nitrogen [55]. The NO formed by the previously described mechanisms can be reduced via its surface reaction with char particles [56]. The detailed equations of the NO_x formation and destruction mechanisms used in this work can be found in [1].

2.2. Economic evaluation methodology

For the evaluation and the comparison of the two investigated cases which represent different technical solutions for the adoption of co-firing at the Meliti PP, the Net Present Value of investment (NPV), the Internal Rate of Return (IRR) and the repayment period of investment are used as criteria.

The Net Present Value (KPA-Net Present Value/NPV) is the sum of all cash flow after taxes deduced in the reference year. It is an indicative of value of money through time. Investments with positive NPV are profitable and favourable. The NPV is calculated according to the equation:

$$\mathrm{NPV} = \sum_{t=0}^{N} \frac{CF_t}{(1+r)^t}, \tag{9}$$

where NPV is the Net Present Value of investment, CF_t is the net cash flow of the investment within period t, r the discount rate (%) and t the time period, which takes values from 0 to N (years). N is the length of the investment.

The Internal Rate of Return (IRR) is defined as the money market rate at which the NPV is zero, which means that the present value of capital investment equals the present value of revenues from the operation. The IRR is calculated from the following equation:

$$0 = \sum_{t=0}^{N} \frac{CF_t}{(1+\mathrm{IRR})^t} \tag{10}$$

The main feature of IRR is that it can be used for investments of different sizes. If the calculated IRR of a project is higher than the discount rate, then the investment is considered as profitable, otherwise the investment is discarded. The higher the IRR, the more profitable the project is.

The repayment period of the investment is the time required to recover the initial investment and can be calculated simply by dividing the initial investment with the net profit/losses. In this work, the repayment period is calculated by taking into account the change in value of money over time.

3. Case studies

Similar to the way of approach in the previous parts, this part is divided in two sections. In the first section the operating and boundary conditions of the CFD simulations are presented and the different cases considered for evaluation are analysed. In the second section the detailed description of the technical solution for each considered case is presented, so that an estimation of capital and operating expenditures for each case is possible.

Generally, two main cases are considered for both CFD modelling and economic analysis:

Case A foresees the delivery of biomass in the lignite yard in the form of pellets. The technical set-up includes facilities for intermediate storage and feeding of biomass to the main lignite conveyor belt. Following that, the biomass fuel is handled by the existing system for lignite, e.g. it passes through the same crushers and mills and enters the boiler through the existing burners without any further optimisation.

In Case B, biomass is delivered to the power plant as baled material or in bulk, as shredded particles. Such forms cannot be handled by the existing feeding system for lignite and thus a need for a dedicated biomass handling line arises. The key point for the CFD simulations is that biomass is milled separately and then transported to the boiler along separate lines; as a result, combustion can be optimised by choosing an appropriate burner level for biomass injection.

Case B can be further subdivided; in Case B1 the injection of the milled biomass takes place in an appropriate level of the existing lignite burner, while Case B2 foresees the installation of

dedicated biomass burners, which allow for further optimisation of the combustion. However, Case B2 requires additional investment and increased technical risks; given the relatively low thermal share of biomass it is not considered further in this study. Fig. 1 shows the different suggested ways of biomass feeding and injection in the boiler considered in the study.

3.1. Description of cases considered for CFD modelling

3.1.1. Cases conditions

In the context of this investigation, the fuel quality, the load of the boiler and the thermal substitution share of lignite from biomass are assumed constant for all the cases examined. The proximate and ultimate analysis of coal and biomass are given in Tables 2 and 3. The lignite characteristics used in the simulations are based on the design lignite data, while the biomass characteristics are based on typical cardoon fuel analysis measured in a laboratory.

The substitution share is set equal to 10% of the reference thermal power input; this value is chosen by the plant operator in order to minimise the potential impacts of the chlorine- and alkali-rich herbaceous biomass combustion in terms of boiler slagging/fouling and corrosion. In addition, this respects the limitations imposed by the local availability of biomass [57], while avoiding a very high specific investment per unit of produced bio-energy which may result when extensive boiler and/or burner retrofit is required. The boiler thermal load considered in this work is the nominal one.

It should be noted that slagging/fouling and corrosion phenomena is not examined by the CFD modelling. Although cardoon exhibits high chlorine, as well as alkalis, content that could cause such issues on dedicated combustion units, the actual chlorine content in the fuel mixture for a 10% thermal share is very low. In addition, the high sulphur content of lignite results in a S/Cl molar ratio much higher than 4, which again indicates non-corrosive behaviour [58].

For CFD modelling a further subdivision of the investigated cases is based on the investigation of (a) the injection points of biomass in the boiler and (b) the mean diameter of biomass particles.

3.1.1.1. Injection points of biomass. The insertion position of biomass is associated with the combustion system simulated. As previously mentioned, in Case A, the biomass is fed along with the lignite in the same already existing belts and subsequently are both pulverized in the lignite mills. In this case the biomass enters the combustion chamber from all burners and all levels, as lignite does. The distribution of cardoon per burner level is assumed to follow that of lignite, as described in the plant operational data.

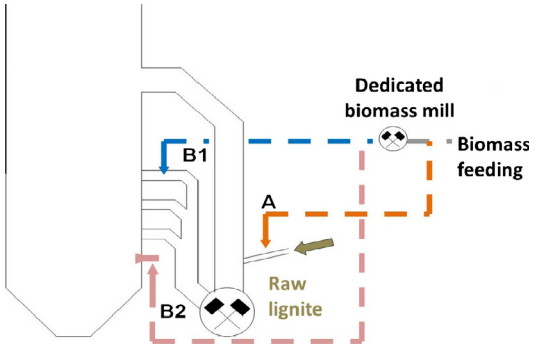

Fig. 1. Cases for biomass injection in the boiler: Case A – "co-milling", Case B1 – dedicated biomass milling/existing lignite burners, Case B2 – dedicated biomass milling/dedicated biomass burners.

Table 2
Proximate analysis of lignite and biomass.

Proximate analysis	Lignite		Biomass	
	wt% (as received)	wt% (after mills)	wt% (as received)	wt% (after mills)
Moisture	36.21	12.00	15.43	5.00
Ash	27.61	38.09	7.30	8.20
Volatile	19.01	26.22	68.94	77.44
Char	17.17	23.69	8.33	9.36
Total	100	100.00	100	100
NCV (MJ/kg)	8.06	12.04	16	16.78

Table 3
Ultimate analysis of lignite and biomass (n.d.: not detected).

Ultimate analysis (wt% dry, ash free)	Lignite	Biomass
C	61.95	50.372
H	4.30	6.742
N	1.65	0.819
O	31.25	41.314
S	0.84	0.258
Cl	n.d.	0.495
Total	100	100

Case B1 corresponds to the installation of a separate milling system for biomass and then to the transportation of the milled biomass through a pneumatic system to the lignite boiler. In this case the pulverized biofuel is injected into the coal duct downstream of the lignite mills and therefore it enters the furnace through the existing lignite burners. In this case, it is possible to choose the level of injection into the coal ducts and the burner level through which the biomass fuel enters. Specifically, Case B1a includes input of entire quantity of biomass through the upper main burners and Case B1b includes input of the entire quantity of biomass through the vapour burners. The input of biomass from the level of the lower main burners is not considered as a case, since a preliminary assessment showed that input of biofuel from this low level only will result in high losses of fuel as unburnt material in the bottom ash.

3.1.1.2. Mean diameter of biomass particles. The mean diameter of biomass particles is a key feature of the combustion system and is strongly related to the system specifications for the biomass grinding system. In order to investigate the effect of the mean diameter of biofuel on its combustion behaviour (temperatures, emissions, char burnout) three cases have been considered with average equivalent diameters of (i) 0.5 mm, (ii) 1.0 mm and (iii) 3.0 mm. The higher biomass particle diameter of 3 mm is not considered for Case B, since the installation of a dedicated biomass milling system is expected to lead to lower particle sizes; hence, this case can be valid only for the non-optimised milling of Case A. It is noted that we have assumed the average equivalent diameter of the biomass particles in the simulation, for simplification reasons, though in reality biomass particles follow a size distribution. In addition, this simplification allows for the derivation of clear conclusions about the effect of the biomass diameter on the operational characteristics of the plant.

On the other hand, the mass weighted distribution of injected lignite particles is presented in Table 4. These values have been derived after taking samples from the existing milling system of the plant.

A short description of the cases examined in this paper is presented in Table 5.

3.1.2. Boiler geometry and boundary conditions

The geometry of the boiler of Meliti power plant and the implemented numerical grid are shown in Figs. 1 and 2. It is important to note that the geometry modelled is in full accordance with the drawings of the plant without the usual geometrical simplifications in similar studies. The purpose of this study is to simulate as accurately as possible the actual operation of the boiler, both for the reference and the co-firing cases (see Fig. 3).

The output of the furnace and the flue gas recirculation zones are modelled setting boundary conditions of Neumann type (first derivative equal to zero). The output mass flow of gas recirculation ducts and furnace outlet is based on thermodynamic calculations in the existing drying and grinding system, according to operational data provided by the operators of the plant. Usually, the flue gas mass flow rate exiting the furnace is in-between 82.4% and 83.4% of the total gas flow inlet, while the rest is driven towards the recirculation ducts in order to supply heat for the fuel drying in the mills. The operating conditions for the reference case and the co-firing ones are listed in Tables 6 and 7. It should be noted that the reference case, for which only lignite is fed to the boiler, is based on the plant design data and their verification by the plant acceptance tests.

3.2. Description of cases considered for economic evaluation

3.2.1. Case A

As mentioned, Case A assumes that cardoon is in the form of pellets by truck from a long-term storage site or directly from the pellet plant to the power plant site. Pellets can be transported within the plant using the existing open lignite feeding conveyor belts, since due to their specific weight, pellet losses during conveying are not expected to be high. In addition, the existing lignite mills are expected to be able to handle the milling of pellets for the investigated level of thermal substitution.

In particular, Case A requires the following key components:

1. The truck delivery and unloading area (bulk pellets transport).
2. The intermediate storage system. First pellets are unloaded in a small size silo, which is located at a lower level for ease of unloading. From there, the pellets are raised through a bucket elevator in a silo for intermediate storage with sufficient capacity to meet the needs for 48 h. The loading of silos and the operation of the bucket elevator will not be continuous but interrupted between each new delivery (1 truck per hour estimated).
3. The feeding system from the silo to the main belt-mixing with lignite. From the intermediate storage silo the pellets are driven through a screw feeder at a weighting belt and from there through a conveyor belt at a distance of 100 m from the silo to the main conveyor belt where it is mixed with lignite. The mixture is led to the coal crushers and then the coal silo. From there it is fed to the mills and then to existing lignite burners.

The following data are considered:

- Daily consumption of biomass: 500 t/day.
- Bulk density of pellets: 600 kg/m^3.
- Required silo storage capacity: $2 * 500/0.6 = 1666.7$ m^3.

Table 4
Mass weighted diameter distribution for lignite particles.

Diameter (μm)	Mass percentage w.w%
300	39.8
170	14.01
90	12.08
50	34.11

Table 5
Short description of the cases examined.

Biomass particle size distribution	Injection methods/cases		
	A	B1 (a) – upper main burners	B1 (b) – vapour burners
i (0.5 mm)	x	x	x
ii (1.0 mm)	x	x	x
iii (3.0 mm)	x		

- Loading of silos and bucket elevator operation: interrupted, after each new delivery of truck (1 truck/h estimated).
- Silo unloading and operation of feeding system and conveyor belt: interrupted according to lignite loading.
- Lignite loading duration: 10 h per day.
- Mass flow of biomass in the feeding system from the feeding silo: 500 t/10 h = 50 t/h or 50/0, 6 = 83.3 m^3/h.

3.2.2. Case B

Case B assumes that the biomass fuel is delivered as bales (50%) or as shredded material (50%). The existing handling system for lignite cannot be used and there is a need for dedicated milling and conveying systems.

In this case, an unloading and delivery area for trucks transporting the biomass in bales or in shredded bulk form is also provided. The case of receiving 50% of the incoming quantity of biomass into bales and 50% in bulk form is considered. The biomass bales are now stored in a covered space, protected from weather conditions, in which there is the capability of loading them with a loader, and an automated bag opening system for the bales. Similarly, in the case of receiving shredded biomass in bulk form, it will be stored in piles inside the storage building or in covered silos with automatic walking floor feeding system.

In particular, this case includes the following components:

1. Truck delivery and unloading area.
2. The intermediate storage system (area near the station entrance). The biomass bales are stored in a covered space, protected from weather conditions, in which there is the capability of loading them with a loader, and an automated bag opening system for the bales. Similarly, in the case of receiving shredded biomass in bulk form, it will be stored in piles inside the storage building or in covered silos with automatic walking floor feeding system. The storage system should be large enough to accommodate enough biomass for 2 days of operation (1000 t).
3. Pretreatment, feeding and grinding of biomass. From the intermediate storage, biomass is transferred to a separate biomass grinding mill where it is pulverized and powdered biomass is stored temporarily and driven pneumatically up to the combustion system.
4. Buffer storage, pneumatic feeding to the boiler. From this intermediate storage, biomass is transferred to a separate biomass grinding mill where it is pulverized and powdered biomass is stored temporarily and driven pneumatically up to the combustion system. Both the buffer silo and the pneumatic feeding systems should follow the APEX standards.

The following data are taken into account:

- Daily consumption of biomass: 500 t/days.
- Mass flow of biomass from storage to mill grinding: continuous 500 t/d/24 h = 20.8 t/h.
- Biomass mill operation: continuous.
- Intermediate storage of powder: buffer for a short time 1–2 h.
- Pneumatic biomass powder feeding up to the combustion system: continuous 20.8 t/h, at a distance of 350 m.

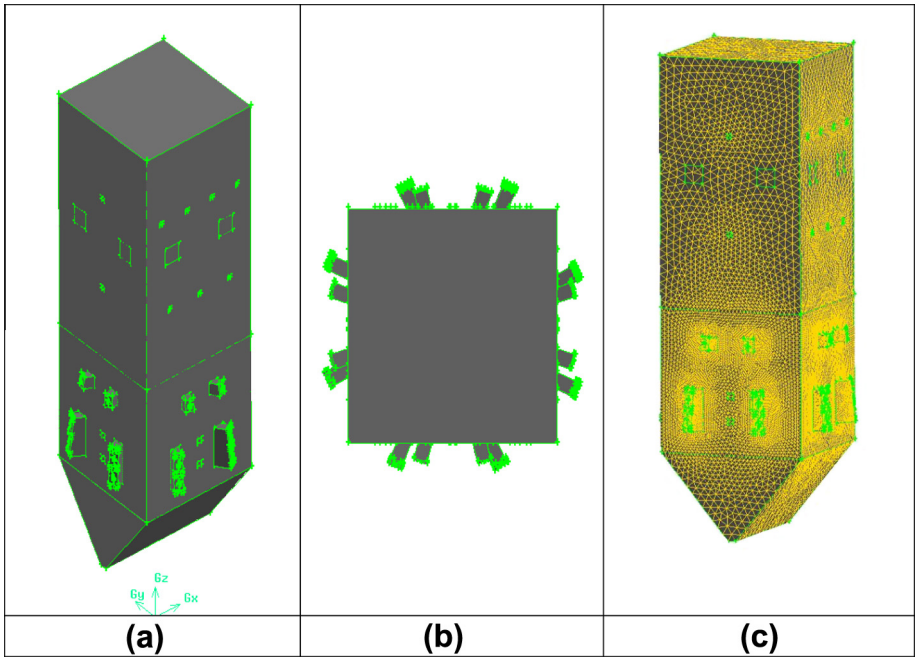

Fig. 2. (a) Geometry of Meliti Boiler, (b) top view of Meliti Boiler and (c) numerical grid.

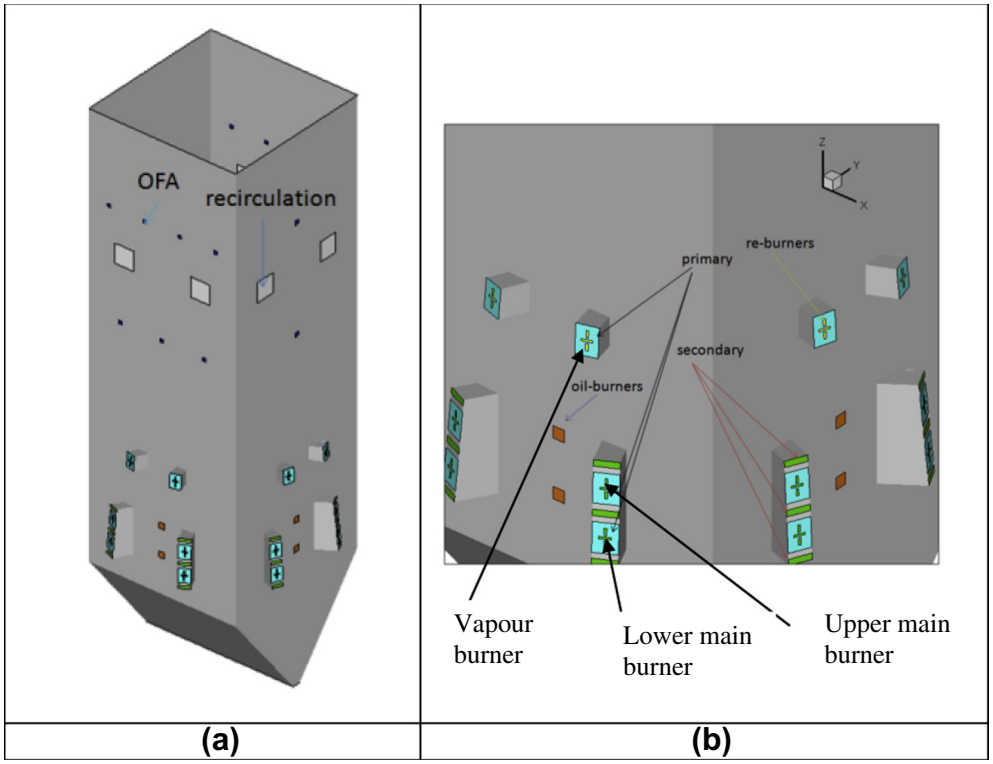

Fig. 3. (a) Over-fire air (OFA) nozzle and recirculation ducts geometry and (b) primary and secondary airstream in the main burners, oil burners and vapour burners geometry.

4. Results and discussion

4.1. Results of technical evaluation (CFD analysis)

4.1.1. Reference conditions

For the reference case, lignite is the only solid fuel entering the boiler; it is injected into six (6) out of the total eight (8) burners. The main furnace parameters for the reference case are presented in Table 8 and compared to design values or data from the plant acceptance tests. More specifically, the furnace outlet temperature is comparable to the design value of 992 °C, while the total heat flux through the membrane walls was found to be 413 MW_{th}. This is in good agreement with a heat transfer of 396.9 MW_{th} estimated by taking into account the following design data and estimates: steam mass flow (282.4 kg/s), inlet and outlet steam data

Table 6
Boiler operating conditions for the reference case.

Stream	Mass flow (kg/s)	Temperature (°C)	Gas composition (wt%)			
			O_2	H_2O	CO_2	N_2
Primary air (transport air)	283.54	220	13.55	16.03	6.83	63.59
Secondary air (from boilers)	164.10	305	23.21	–	–	76.79
Secondary air (by stage combustion system)	66.37	305	23.21	–	–	76.79
Secondary air (from ash hopper)	11.52	151	23.21	–	–	76.79
Lignite	117.0	100	–	–	–	–
Biomass	–	–	–	–	–	–

Table 7
Boiler operating conditions for co-firing with 10% biomass thermal share.

Stream	Mass flow (kg/s)	Temperature (°C)	Gas composition (wt%)			
			O_2	H_2O	CO_2	N_2
Primary air (transport air)	272.92	220	13.91	15.26	6.63	64.20
Secondary air (from boilers)	162.83	305	23.21	–	–	76.79
Secondary air (by stage combustion system)	65.86	305	23.21	–	–	76.79
Secondary air (from ash hopper)	11.43	151	23.21	–	–	76.79
Lignite	105.3	100	–	–	–	–
Biomass	6.42	100	–	–	–	–

(316 °C/268.7 bar and 418 °C/258.1 bar respectively) and 3% radiation losses for the total steam production of the boiler (870 MW_{th}). The O_2 and NO_x concentration values for the reference case are also in line with the plant acceptance tests and the typical values of operation under full-load conditions (O_2: 2.9 wt% compared to 2.79 wt%, $NO_x \sim 254$ mg/N m^3 compared to 200 mg/N m^3, both at 6 vol.% dry O_2). From this comparison, it is evident that the numerical model predicts quite well the main operational characteristics of the power plant, thus allowing us to proceed with the examination of the co-firing concepts.

4.1.2. Co-firing simulations – investigation of the biomass particle size for Case A

The basic operating parameters, as obtained numerically for cases A (i), A (ii) and A (iii) are also presented and compared to the reference case in Table 8. Based on the results, no significant operational changes are expected to occur in the boiler characteristics, except for an increase of around 4% in the thermal flux towards the membrane walls. The concentration of NO_x varies by up to 8% with a decreasing trend, showing that the recovery of lignite with biomass has a positive impact on NO_x emissions. Table 9 shows the efficiency of the furnace that is calculated based on the wet and solid ash losses.

Fig. 4, depicts the distribution of the mean temperature along the height of the boiler being developed for the reference and cases A (i), A (ii) and A (iii). As can be seen, the mean temperature is practically the same for all examined cases for heights higher than 20 m. At lower heights, higher temperatures are observed compared to the reference case as the biomass particle size increases; the mean temperature of Case A (iii) at a height of 12 m is 500 °C higher compared to the reference case. This is due to the shift of the volatile release and combustion section of the furnace to lower heights as the biomass particle size increases. These local hot spots could cause problems in the boiler operation if the substitution share is much higher than 10% and should be studied in depth in the future.

The total lignite and biomass char burnout are respectively presented in Figs. 5a and 5b, both for the whole volume of the boiler and for the particles exiting the furnace top and hopper. Furthermore, Figs. 6a and 6b present the mass flow percentage of lignite and biomass particles exiting the boiler outlet and hopper for each burner level. The rest of the fuel particles are exiting the boiler through the recirculation ducts.

From these graphs the following conclusions can be extracted:

- The lignite and biomass entering from vapour burners (re-burners) exit through the furnace outlet with a percentage of approximately 87%, while the rest passes through the recirculation ducts regardless of the particle size of biomass.
- The percentage of the lignite particles from the lower burners that exit the furnace through the hopper increases to 28.4% for Case A (i) and 29.08% for Case A (ii) compared to 26.3% for the reference case; a decrease to 24.47% is observed for Case A (iii). For cases A (i) and A (ii) it appears that the lower flue gas velocities in the hopper allow for increased lignite particle losses; for Case A (iii) the high temperature increase in the hopper area compensates for the reduced flue gas flow and results in higher velocities and, therefore, to a reduction of lignite particles that fall on the ash hopper.
- The corresponding percentage for biomass leaving the ash hopper increases significantly for Case A (iii) (Reference case: 0%, Case A (i): 0.21%, Case A (ii): 0.74%, Case A (iii): 31.25%), suggesting that the diameter of 3 mm presents significant ash hopper losses and therefore should be avoided as an operating case.
- Note that the biomass char burnout is significantly reduced as the diameter increases, particularly for biomass particles entering from the upper and lower main burners.

From these results one can conclude that Case A (iii) should be avoided since it results in significant mass and energy losses of solid particles in the bottom ash, while these losses are significantly greater for the lower burners in comparison with the upper.

Table 8
Comparison of main furnace parameters between design data, reference and co-firing cases.

Case	Temperature (°C)	O_2 (wt%)	CO_2 (wt%)	Total heat flow through membrane walls (MW_{th})	NOx mg/N m^3 (6 vol.% dry)
Design data/ acceptance tests	992	2.79	20.0	396.9	<=200
Reference	983	2.90	19.48	412.97	253.8
A (i) – 0.5 mm	993	3.32	19.55	434.60	234.8
A (ii) – 1.0 mm	987	3.46	19.40	427.90	242.9
A (iii) – 3.0 mm	985	3.52	19.40	428.55	233.86
B1a (i)	995	3.08	19.82	443.19	257.96
B1b (i)	1005	3.08	19.83	441.18	212.76
B1a (ii)	991	3.14	19.74	443.78	246.2
B1b (ii)	1000	3.14	19.74	434.97	231.2

Table 9
Furnace performance based on combustion efficiencies for ash losses.

	Combustion efficiency based on fly ash losses (%)	Combustion efficiency based on wet ash losses (%)	Weighted combustion efficiency based on wet and fly ash losses (%)
Reference	99.94	84.24	97.32
A (i) – 0.5 mm	99.90	89.14	98.13
A (ii) – 1.0 mm	99.86	85.57	97.41
A (iii) – 3.0 mm	99.13	84.56	96.96
B1a (i)	99.96	93.34	99.07
B1b (i)	98.49	94.50	98.11
B1a (ii)	99.95	93.14	99.00
B1b (ii)	98.03	91.27	97.11

Fig. 7 shows the contours of temperature in the vertical plane passing crossing the centre of the boiler ($X = 0.0$), and the total heat flux on membrane walls. Fig. 8 presents the ratio of the radiative heat flux to the total heat flux; as can be seen, the heat leaving the furnace through the membrane walls is mostly due to radiation, as is expected of such boiler types. Fig. 9 shows the temperature and velocity distributions and concentrations of NO_x at the burner levels.

Therefore a 10% thermal substitution share does not significantly affect the proper operation of the boiler in terms of the developing temperature fields and NO_x emissions, except for the Case A (iii) (3 mm), where biomass losses from ash hopper are quite high.

4.1.3. Co-firing simulations – investigation of the biomass particle size for injection at different burner levels (Cases B1a and B1b)

4.1.3.1. Case (i) – 0.5 mm: Cases B1a (i) and B1b (i). Table 8 presents the basic operating parameter values for these cases compared to the reference one. From the table it is shown that the boiler operation is not significantly affected in any case with 10% substitution of thermal power from biomass, except for the fact that there is an increase in the total membrane wall heat flux of about 7% and a significant NO_x reduction by around 16.2% in the case of injecting biomass from the vapour burners.

In these cases, the mixed combustion improves the efficiency of the furnace. Fig. 10 depicts the mean temperature spatial distribution in the boiler for reference Case A (i), B1a (i) and B1b (i).

For these cases no significant changes in the boiler operation are expected when biomass enters the furnace through individual fuel inlets (upper main and vapour burners). As the height of biomass injection increases, the position of the hot spots are developing in higher heights (the difference in temperature at 12 m for cases A (i) and B1b (i) is about 550 °C). Thus, the biomass injection from one burner level is not optimal for maintaining the flame temperature uniform throughout the entire furnace height range, especially if the thermal share substitution is much higher than 10%. In Figs. 11a and 11b, the total lignite and biomass char burnouts are presented. Furthermore, Figs. 12a and 12b present the mass flow percentage of lignite and biomass solid particles exiting the boiler outlet and hopper per burner level.

From the afore-cited graphs the following conclusions can be extracted:

- For cases where biomass enters the furnace in specific burners (either the upper main ones or the vapour burners) the lignite char burnout is improving compared to the case of biomass entering from all the three burner levels.
- In each of the cases studied, the amount of lignite leaving the ash hopper is decreasing, when it enters from the lower main burners (Case A (i): 28.41%, Case B1a (i): 23.82%, Case B1b (i): 21.47%) and upper main burners (Case A (i): 4.19%, Case B1a (i): 3.16%, Case B1b (i): 1.33%), improving the combustion quality of the boiler. This suggests reduced possibility for unburnt lignite losses in the hopper.
- In the case when biomass enters through the upper main burners only (B1a), there is a little increase in the amount of biomass leaving the outlet, while if the biomass comes from vapour burners only (B1b) the amount is reduced. For both cases the ash hopper losses are minimal for biomass.

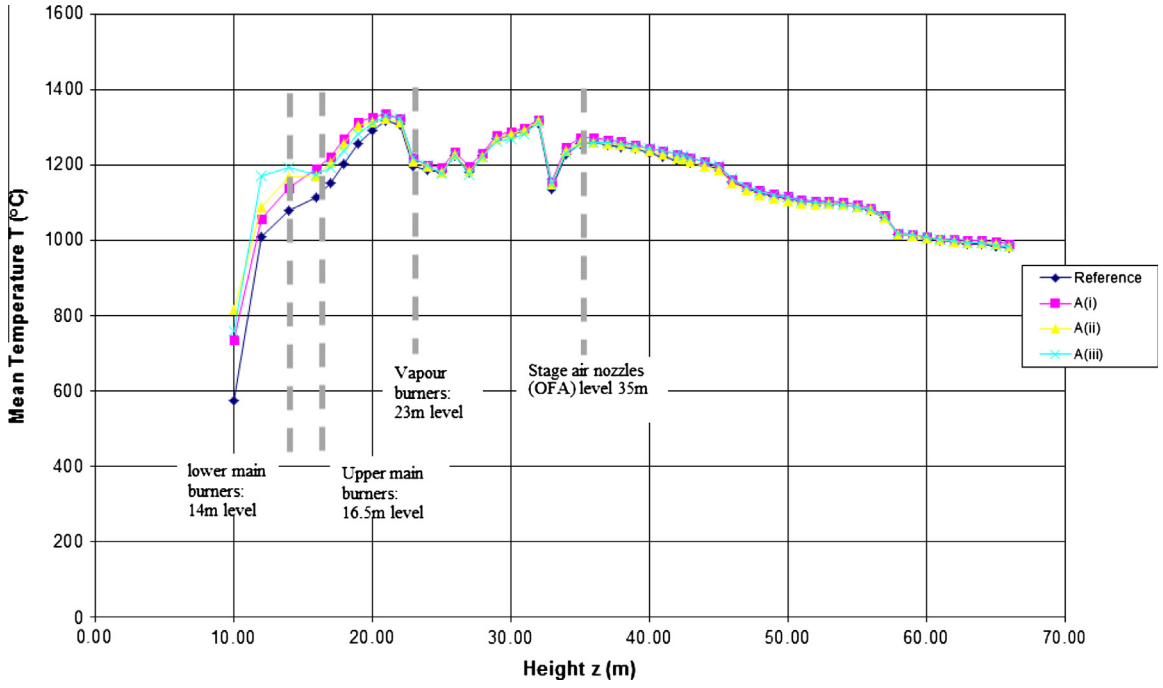

Fig. 4. Distribution of mean temperature along the boiler height for the reference case, A (i), A (ii) and A (iii).

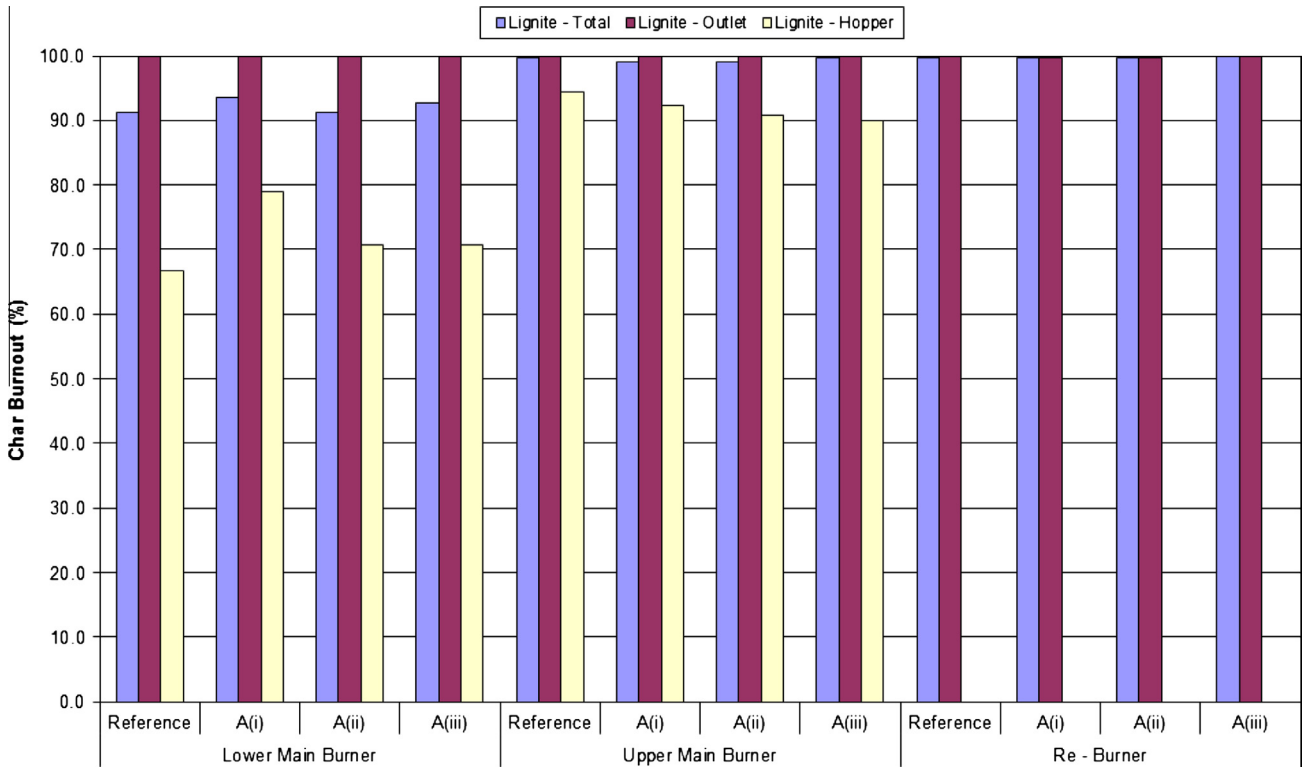

Fig. 5a. Lignite char burnout per burner level, overall, at output and at ash hopper of the boiler.

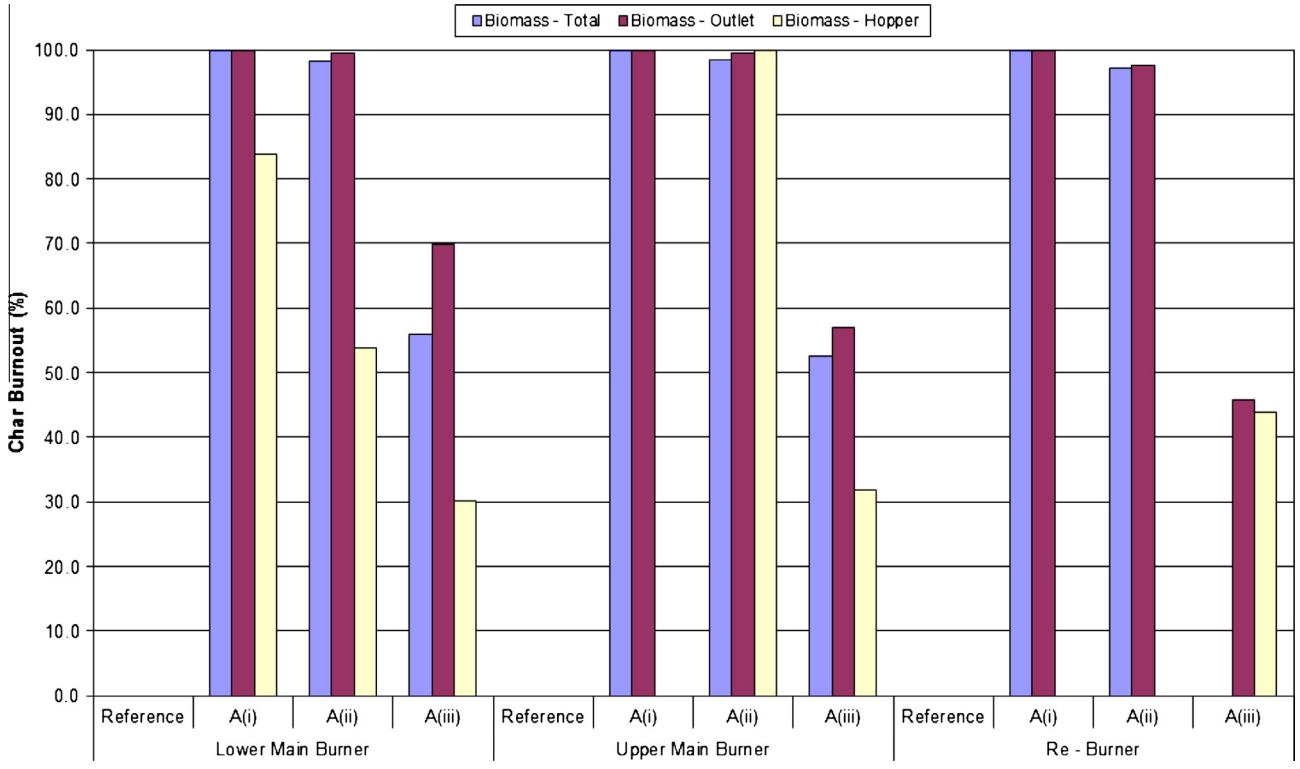

Fig. 5b. Biomass char burnout per burner level, overall, at output and at ash hopper of the boiler.

To conclude, the combustion behaviour of biomass is not changing significantly, while the behaviour of lignite both in terms of burnout and ash hopper losses is improving, making the B1b case the best to choose among all the examined. The

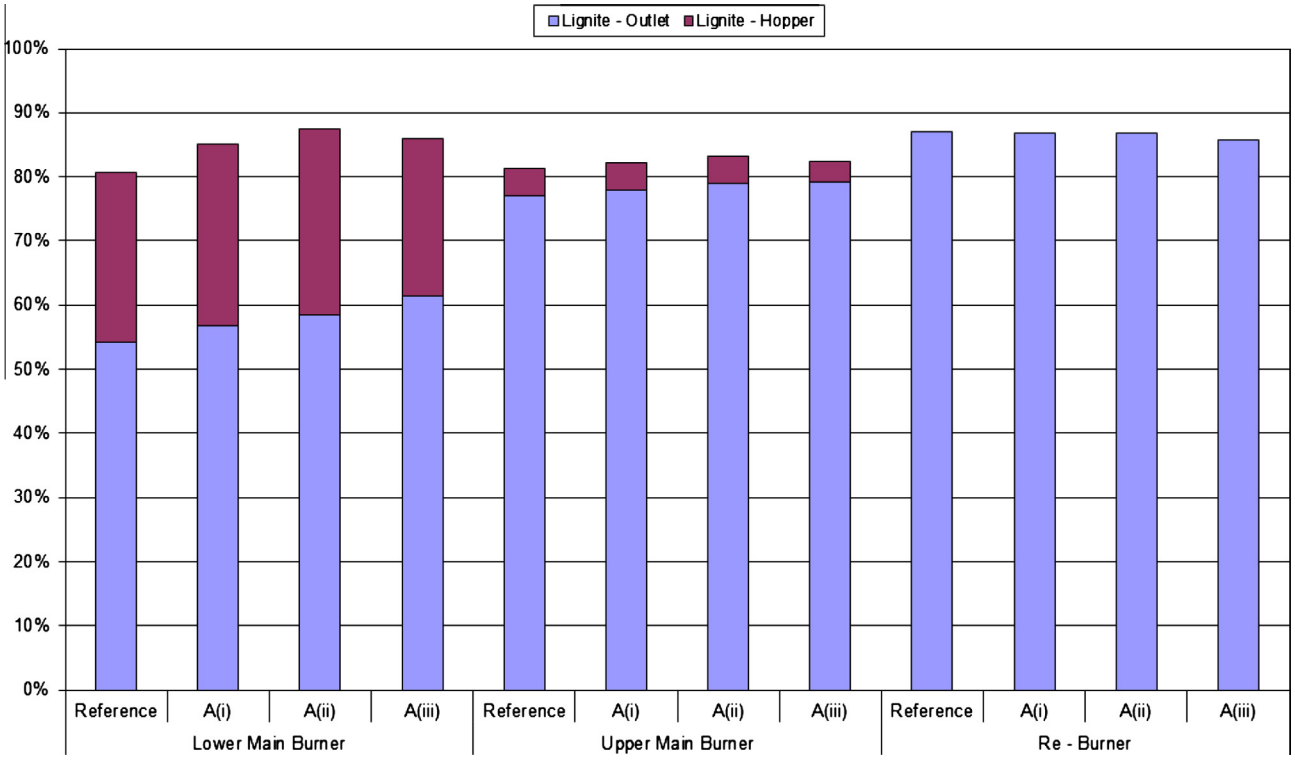

Fig. 6a. Mass percentage of lignite particles leaving the outlet and the ash hopper of the boiler per burner level.

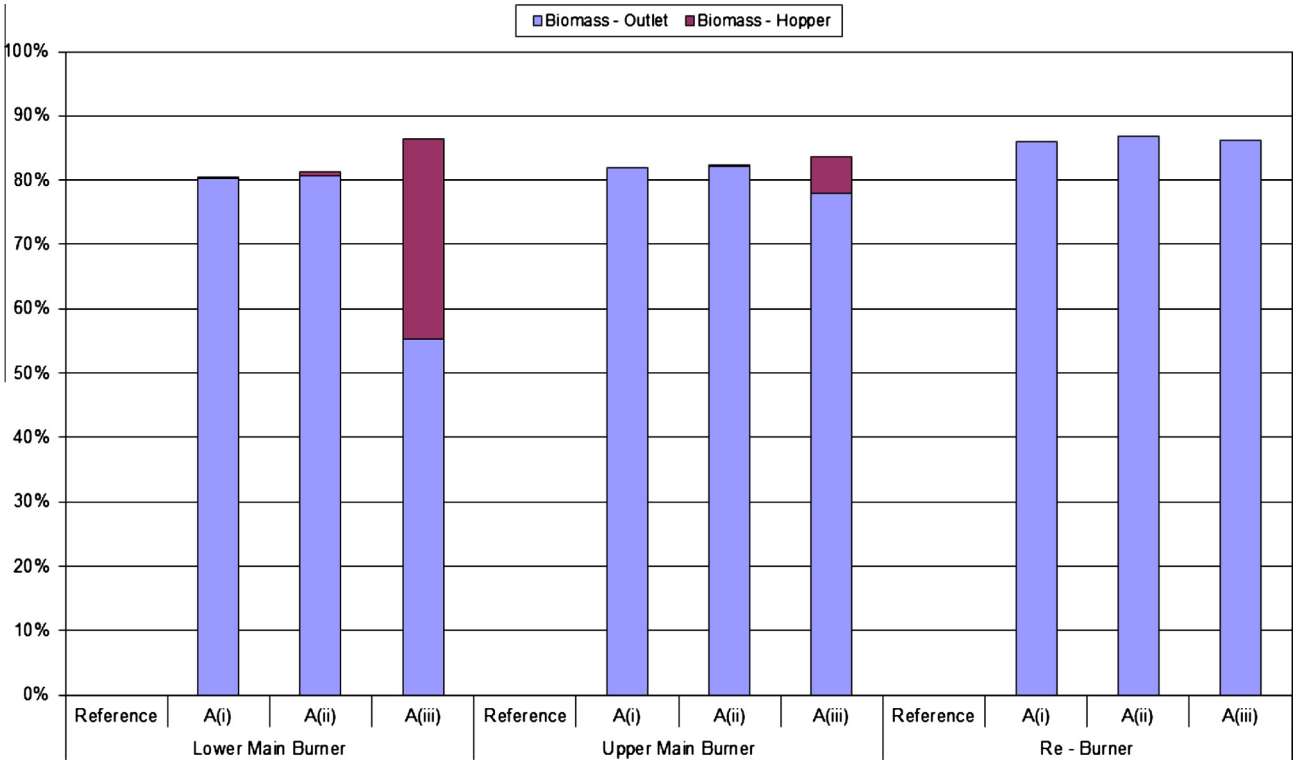

Fig. 6b. Mass percentage of biomass particles leaving the outlet and the ash hopper of the boiler per burner level.

selection of Case B1b as the optimal one is also supported by the significant reduction in the NO_x concentration. Despite the observed temperature increases and the expectations for increased thermal NO_x formation, the main reason for the decrease

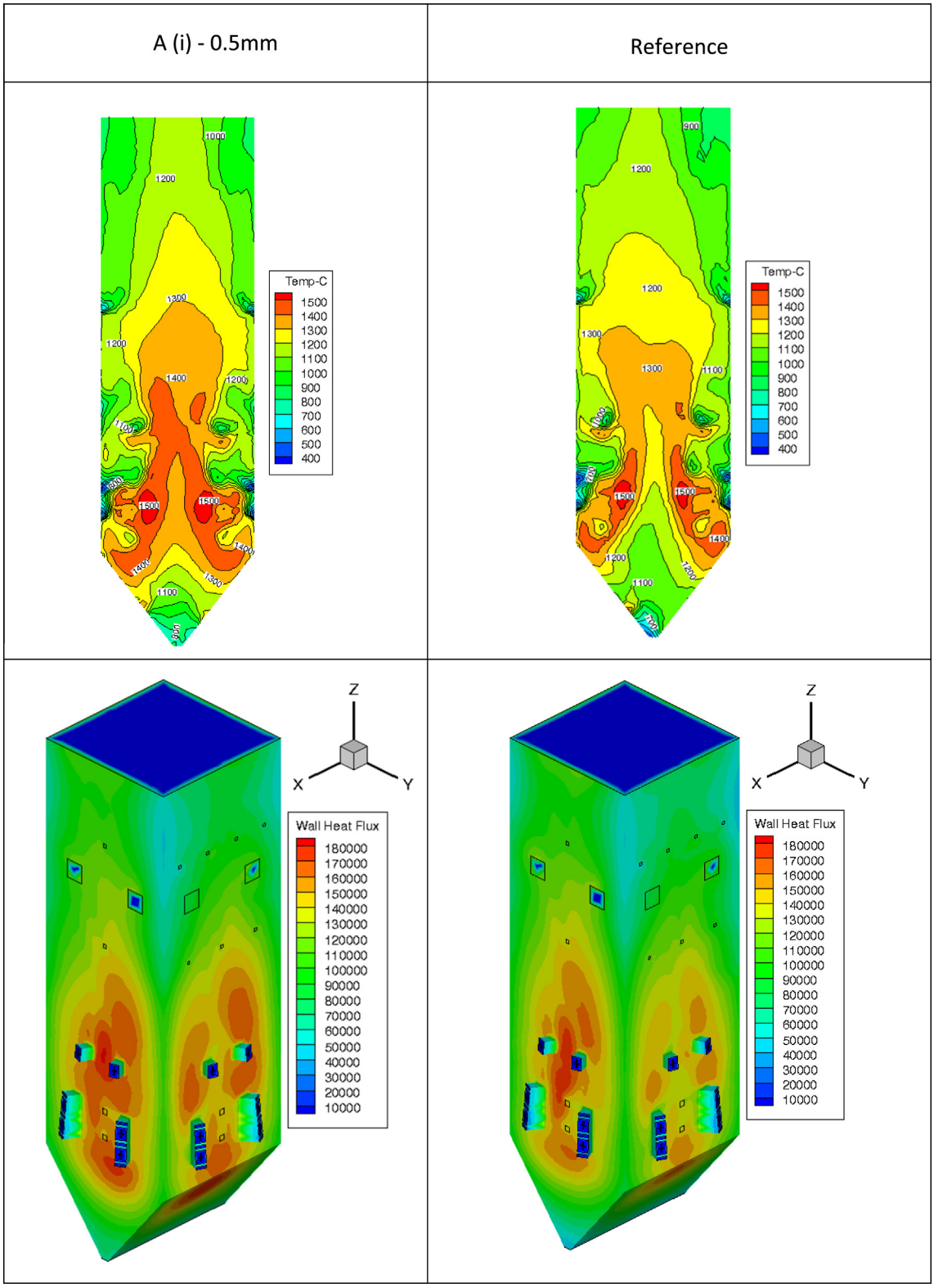

Fig. 7. (a) Contours of temperature on the vertical plane and (b) heat flux on walls, for cases A.

of the total NO_x emissions during biomass co-firing is the high decrease of fuel NO_x due to the different intermediate species paths for the two fuels. As discussed in detail in Section 2.1.3, NH3 and HCH are the main intermediate species during biomass and lignite N-conversion respectively; the former leads to lower fuel NO_x over the latter.

4.1.3.2. Case (ii) – 1.0 mm: Cases B1a (ii) and B1b (ii). The mean diameter in this investigation is 1.0 mm. Tables 8 and 9 present the basic operating conditions and furnace performance for cases B1a (ii) and B1b (ii) compared to the reference one. Again the boiler operation is not significantly affected, except for the fact that there is an average increase in total heat flux through membrane

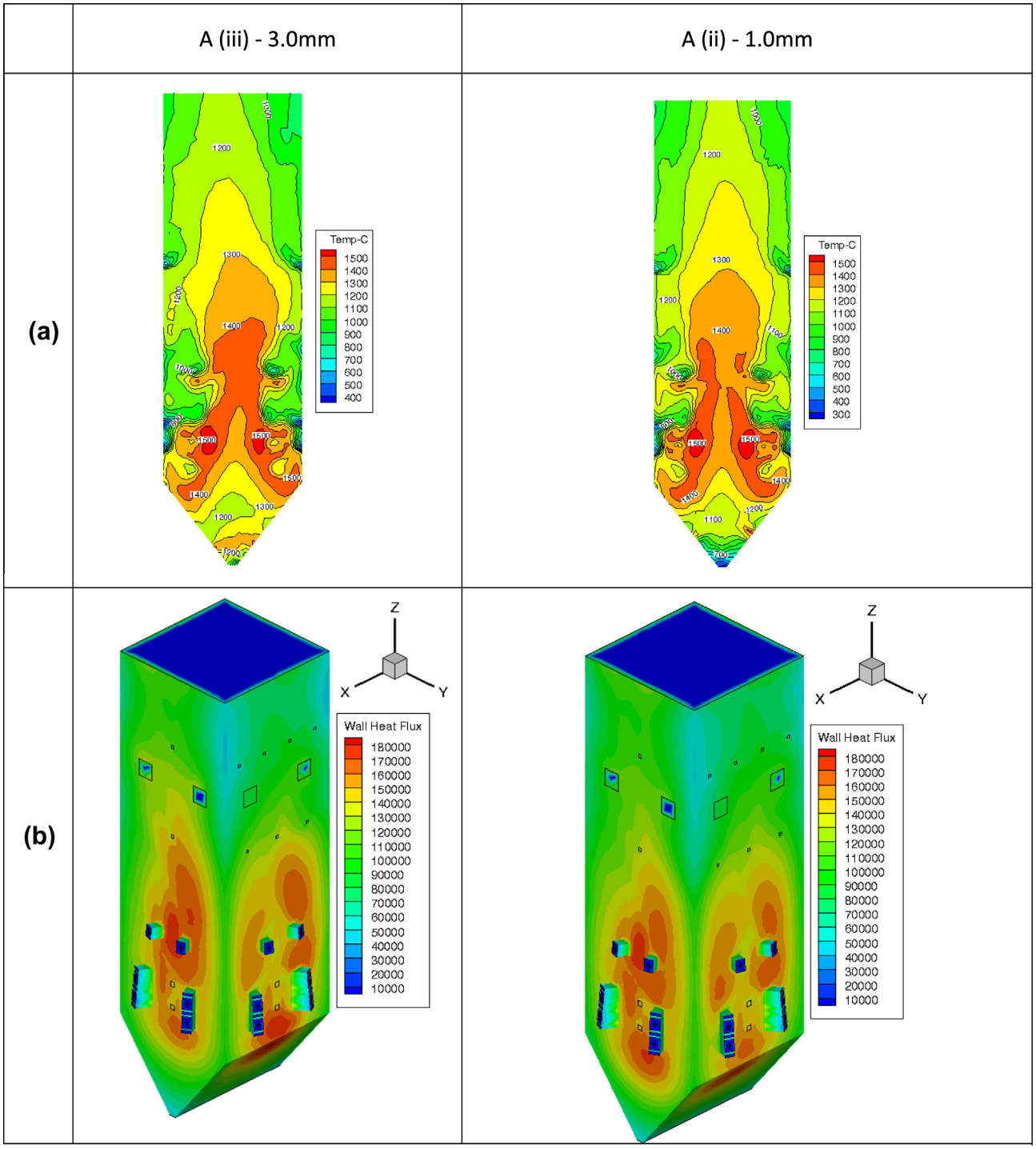

Fig. 7. (*continued*)

walls by approximately 6.5% and a significant reduction of up to 8.7% in the NO_x emissions when increasing the biomass injection height. The increased heat flux towards the membrane walls is justified by the lower flue gas mass flow rate for the co-firing cases compared to the reference case, coupled with the fact that the flue gas temperature at the outlet of the furnace is not increasing significantly. Therefore, the enthalpy of the flue gas at the furnace exit is lower and since the thermal input remains the same, the energy balance requires that the heat flux towards the membrane walls is higher in the co-firing cases.

In these cases mixed combustion also improves the efficiency of the furnace. Fig. 13 shows the distribution in height of the average temperature in the boiler being developed for the reference operation, Case A (ii), B1a (ii) and B1b (ii). The aforecited graph reveals that the induced temperature field follows the same behaviour with the corresponding of cases (i). The tendency of the phenomenon to present a delayed development of hot temperature spots is not significantly affected and differentiated between case (i) (0.5 mm) and case (ii) (1.0 mm).

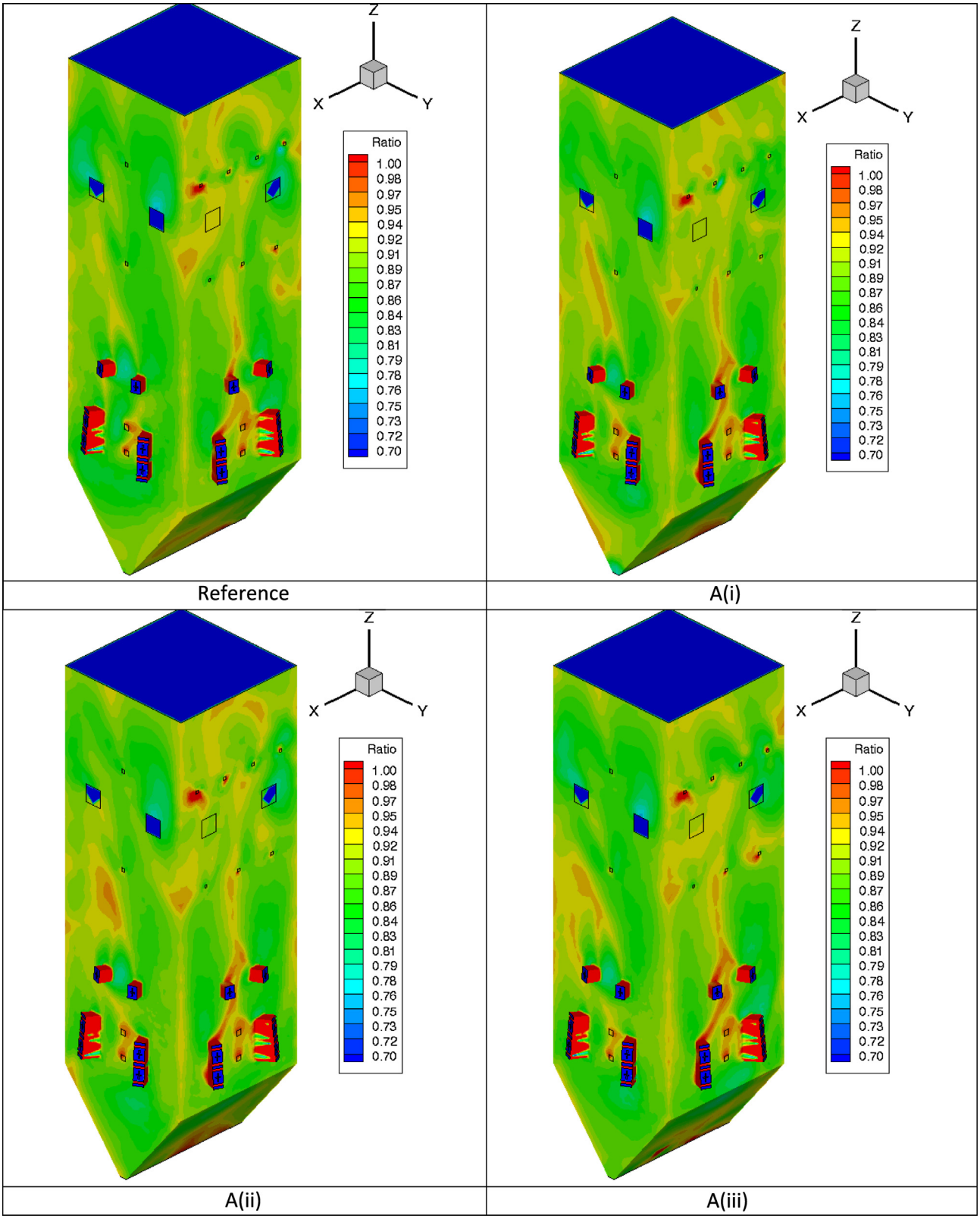

Fig. 8. Radiative heat flux to total heat flux on membrane walls for cases A.

Figs. 14a and 14b present the total lignite and biomass char burnouts. Furthermore, Figs. 15a and 15b present the mass flow percentage of lignite and biomass solid particles exiting the boiler outlet and hopper per burner level.

From these graphs the following important conclusions can be extracted:

- For cases where the biomass enters only from the upper main burners, an improved lignite char burnout is clear compared to the case of biomass entering from all the three burner levels. When the biomass enters through the vapour burners, lignite burnout slightly decreases.

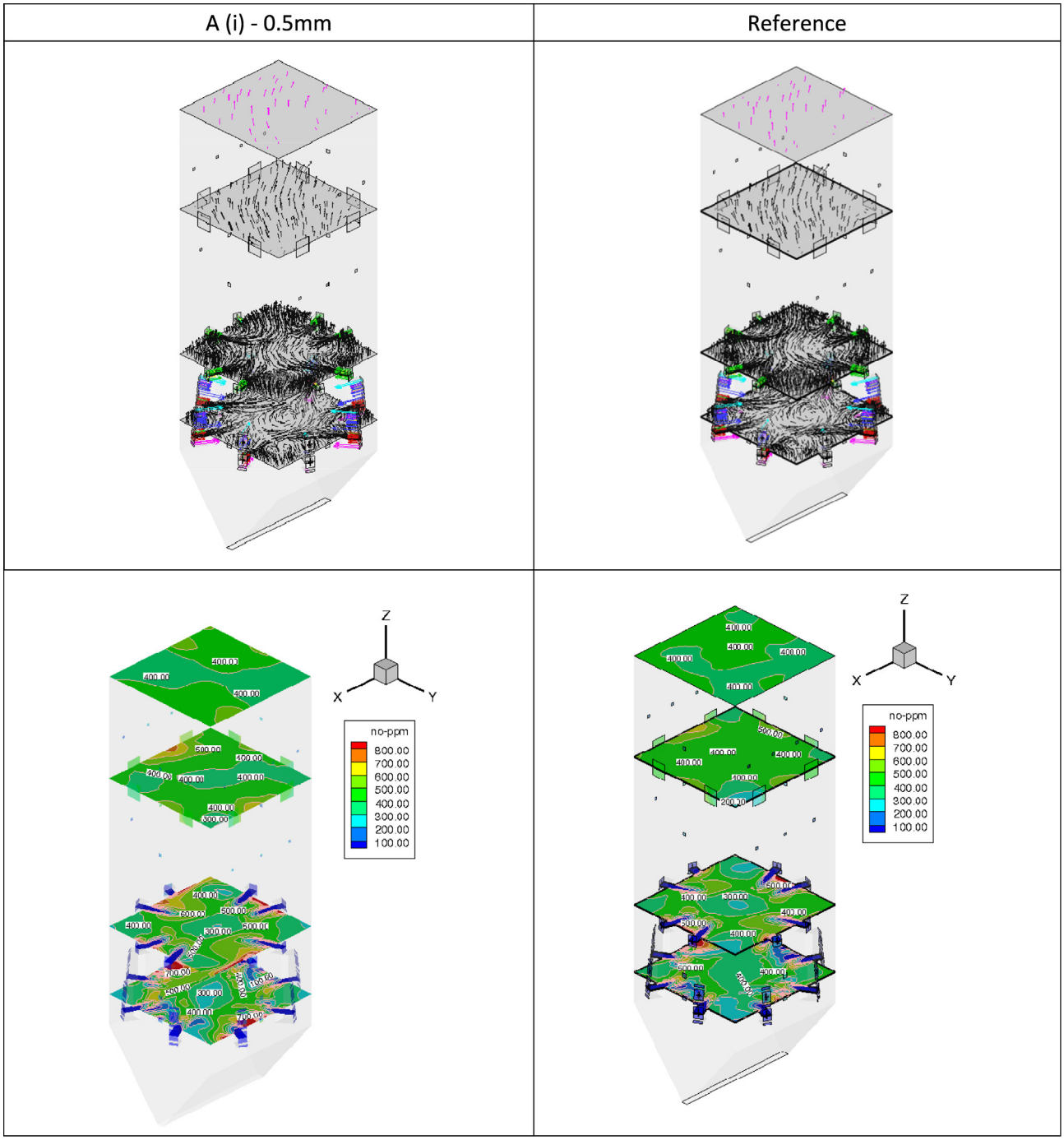

Fig. 9. (a) Induced velocity field (m/s) and (b) NOx concentration spatial distribution at burner levels for cases A.

- The amount of lignite leaving the ash hopper is reduced when entering from the lower main burners (Case A (ii): 29.08%, Case B1a (ii): 24.60%, Case B1b (ii): 24.20%) and upper main burners (Case A (ii): 4.17%, Case B1a (ii): 3.74%, Case B1b (ii): 2.63%). This suggests reduced possibility for unburnt lignite losses in the hopper.
- In Case B1a (ii) (entrance from upper main burners), there is little increase in the amount of biomass leaving the outlet but significant reduction in the burnout of biomass exiting the hopper (Case. A (ii): 100%, Case B1a (ii): 93.43%). In Case B1b (entrance from vapour burners), the amount of biomass leaving the outlet decreases (Case A (ii): 86.88%, Case B1b (ii): 84.11%). For both cases the ash hopper losses are small for biomass, just as in the previous operating cases (i).

To conclude, the combustion behaviour of biomass in these cases does not change significantly, while the behaviour of lignite both in terms of burnout and ash hopper losses are highly improved. For Case B1a (ii) however, where biomass enters through the upper main burners, ash hopper losses are increased by 0.07% along with a significant decrease in the biomass burnout. Therefore Case B1b (ii) is considered preferable compared to B1a (ii).

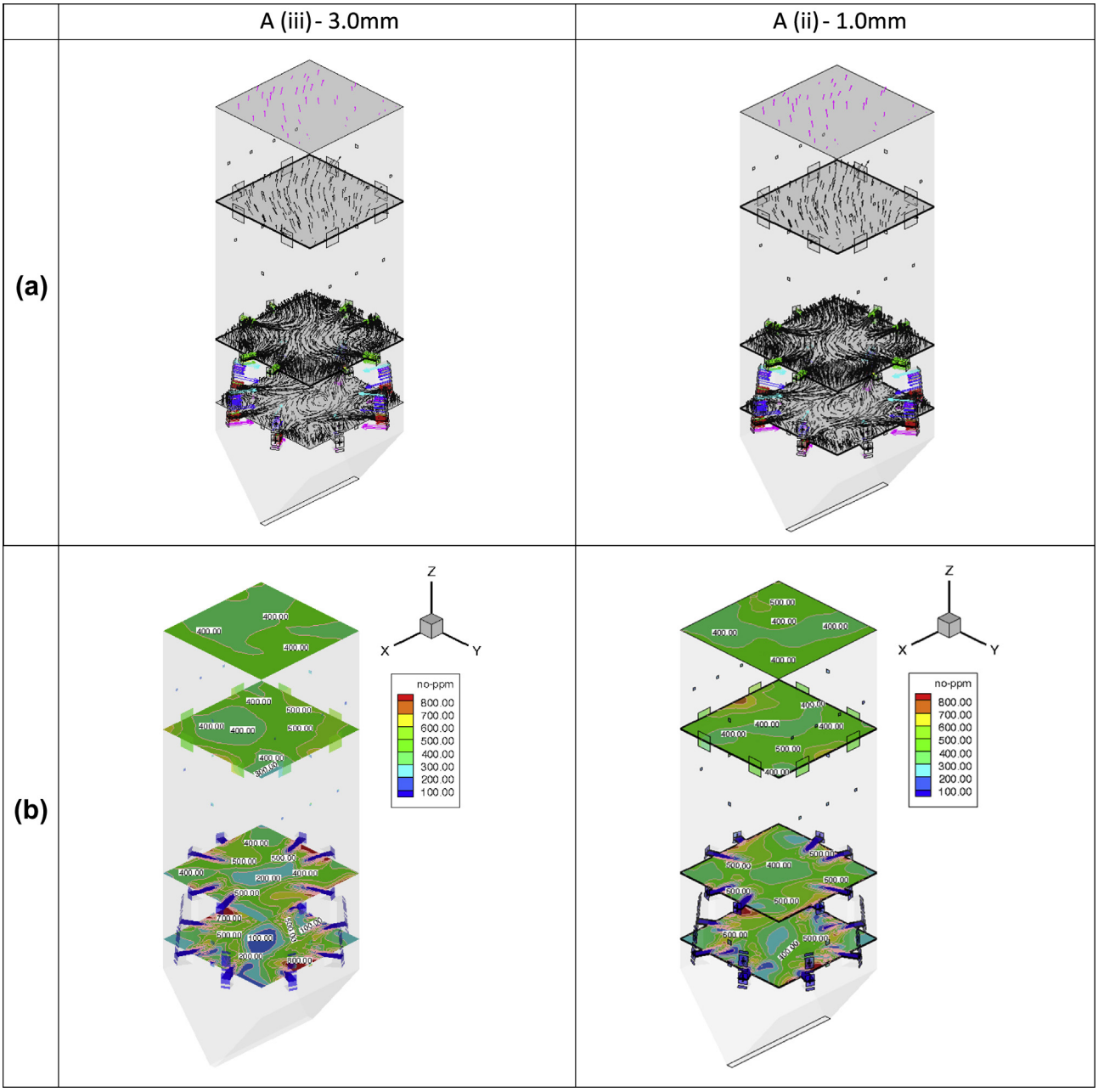

Fig. 9. (*continued*)

All the aforementioned predictions indicate that biomass should be entering the boiler with a mean diameter between 0.5 and 1 mm, so that combustion without significant losses can be maintained. Nevertheless, the most optimal selection of operation is for biomass to be injected from the vapour burners.

4.2. Results of economic evaluation

4.2.1. Estimation of expected costs and revenues from the application of co-firing cases

The difference in Net Present Value of each investment in relation to the case of non-mixed combustion is affected by:

- Additional capital and operating expenses due to the operation of co-firing systems. These costs include: (a) Investment cost, (b) The difference in fuel costs due to the change of fuel, and (c) the additional costs of operation and maintenance, personnel, etc.
- The additional revenue/savings generated by biomass co-firing. It includes: (a) the increased revenues from electricity generation due to the biomass feed-in tariff and (b) the savings from CO_2 emission savings.

4.2.1.1. Total cost of investment. The Total Plant Cost (TPC) includes design costs, procurement costs and construction costs. For co-firing, a wide range of 100–600 USD/kW_e is reported [59], depending on the fuel and technical solutions adopted. Projects

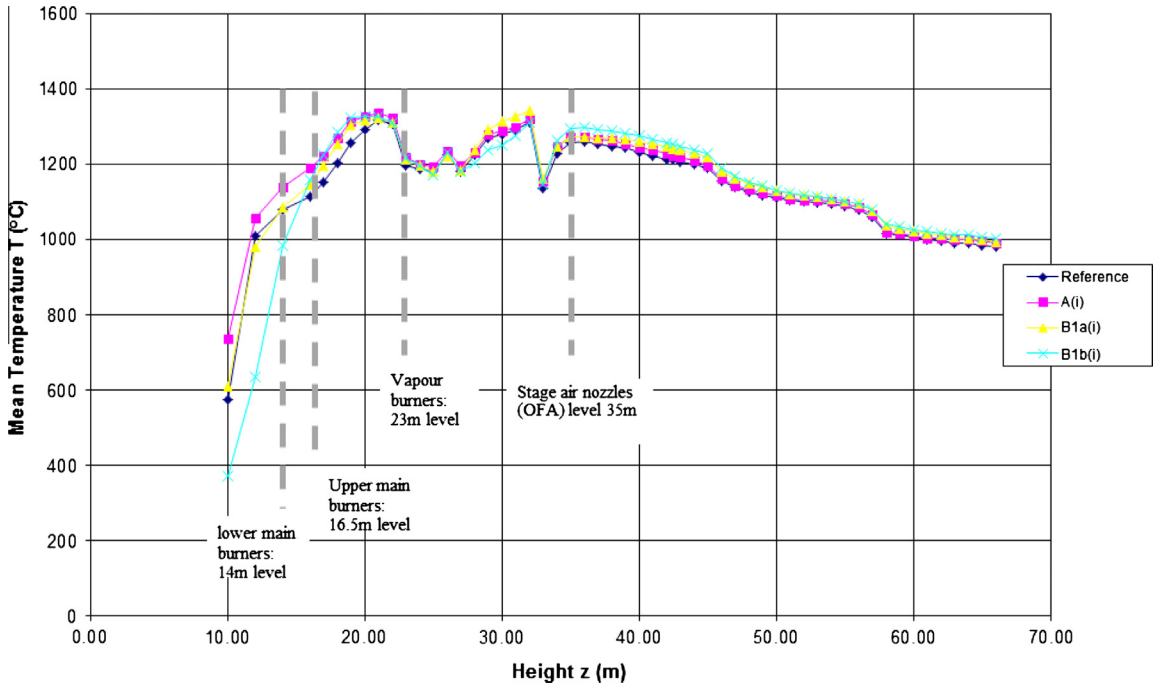

Fig. 10. Distribution of average temperature of the boiler in height for the reference case, A (i), B1a (i) and B1b (i).

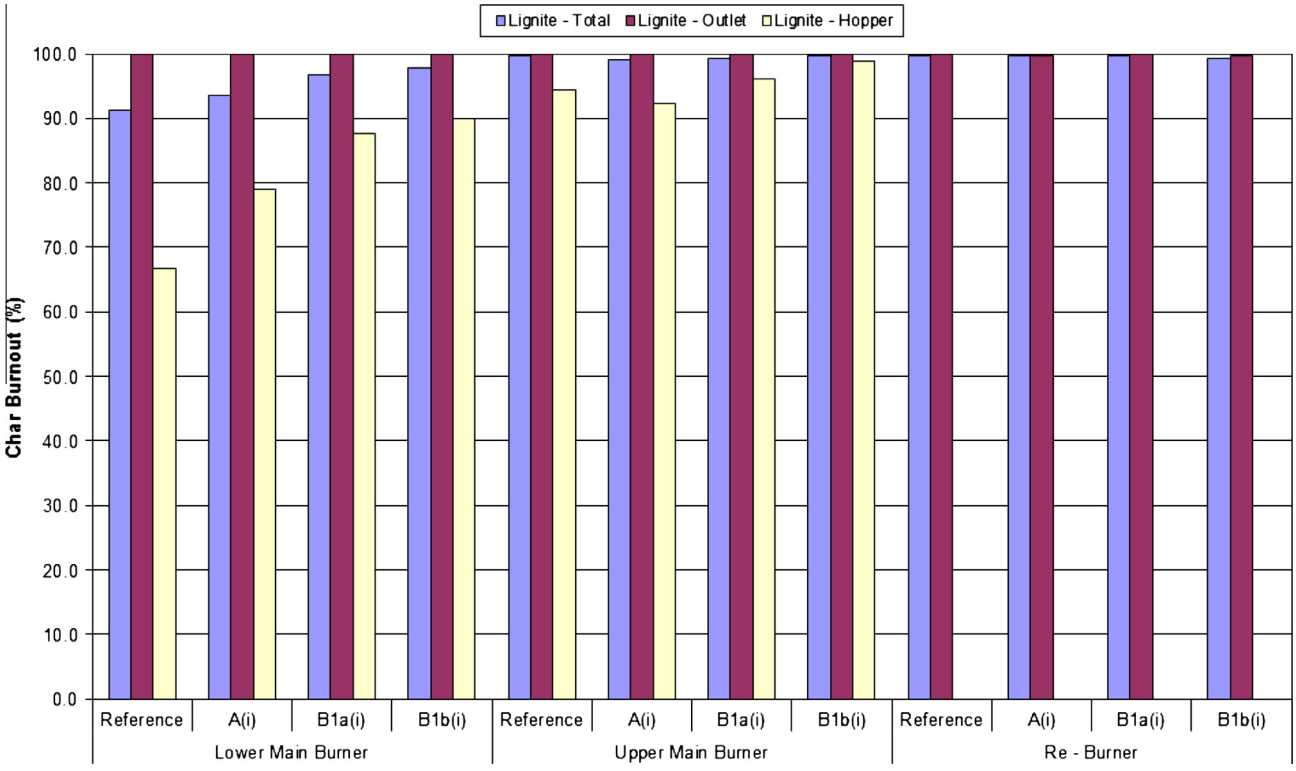

Fig. 11a. Lignite burnout per burner level, overall, at furnace outlet and at ash hopper.

that implement modest technological solutions and minimal modifications in the boiler section require much lower specific costs compared to ones where extensive boiler retrofitting is required. In any case, these values are much lower compared with the corresponding specific costs of new facilities of 100% dedicated biomass combustion, which may reach 2500–3000 €/kW$_e$. This significant difference in cost is due to existing equipment used in the case of co-firing.

In this work, the required TPCs for the implementation of Cases A and B is based on economic offers received by the plant

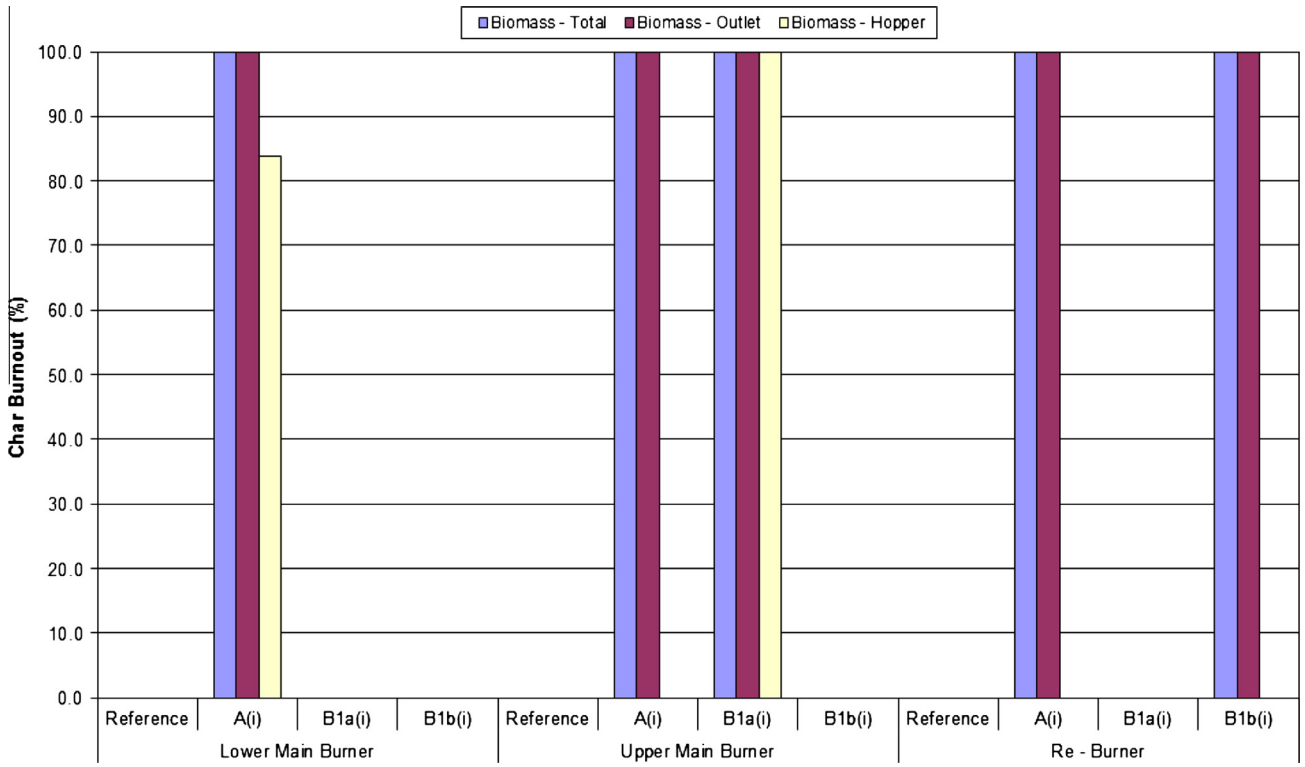

Fig. 11b. Biomass char burnout per burner level, overall, at furnace outlet and at ash hopper.

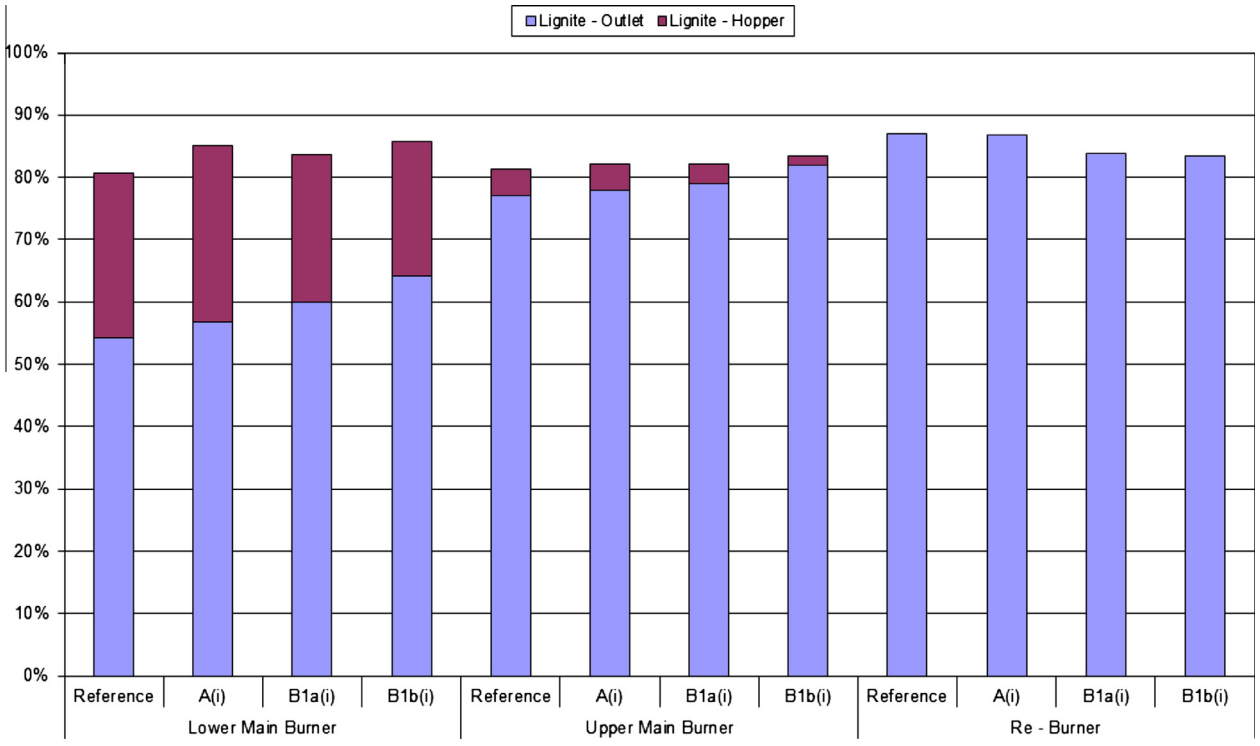

Fig. 12a. Mass percentage of lignite particles leaving the outlet and the ash hopper of the boiler per burner level.

operator for the technical specifications described in Section 3.2. The economic evaluation is based on the Total Cost of Investment (TCI), also known as the Capital Expenditure (CAPEX), which is calculated by increasing the TPC by 5% for development costs and by a further 10% as additional unplanned costs. The TCI is given in Table 12 and amounts to 15.6 €/kW_e for Case A and 41.7 €/kW_e for Case B. As explained, these low values are justified by the lack of any boiler retrofitting. It should be noted that the

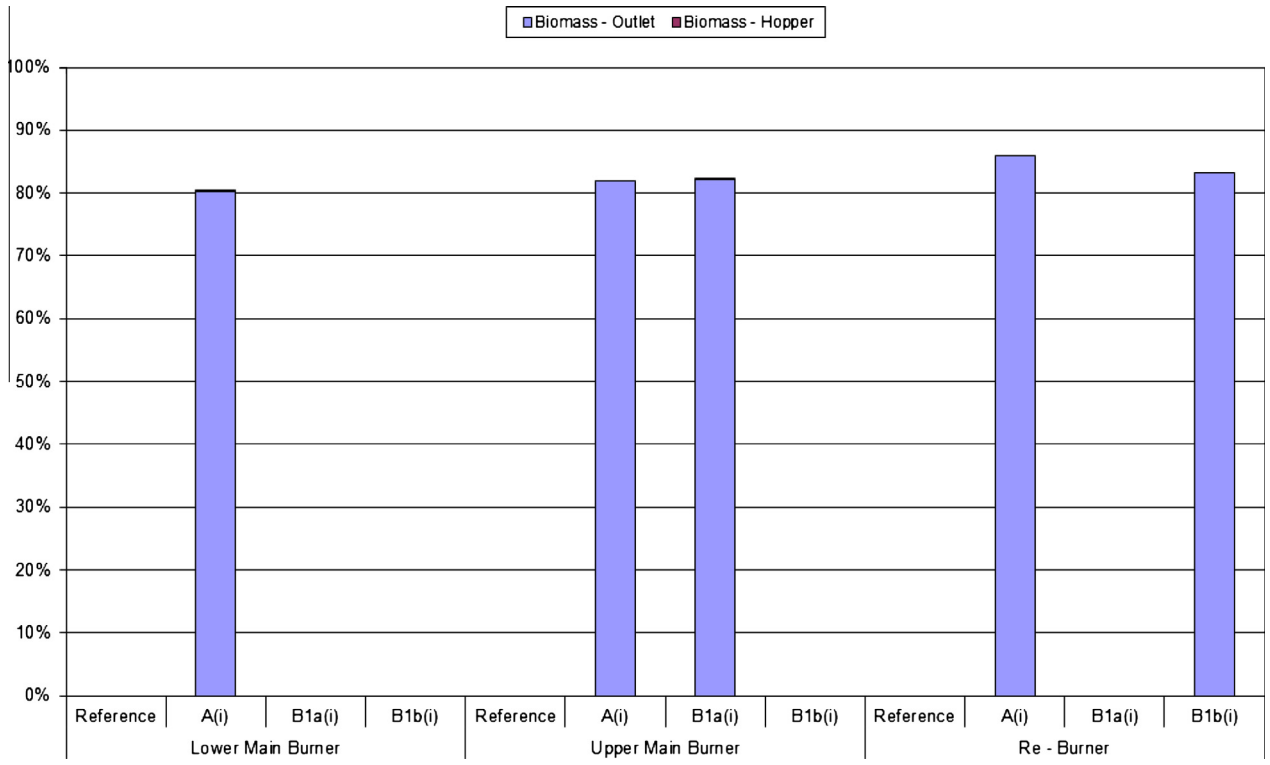

Fig. 12b. Mass percentage of biomass particles leaving the outlet and the ash hopper of the boiler per burner level.

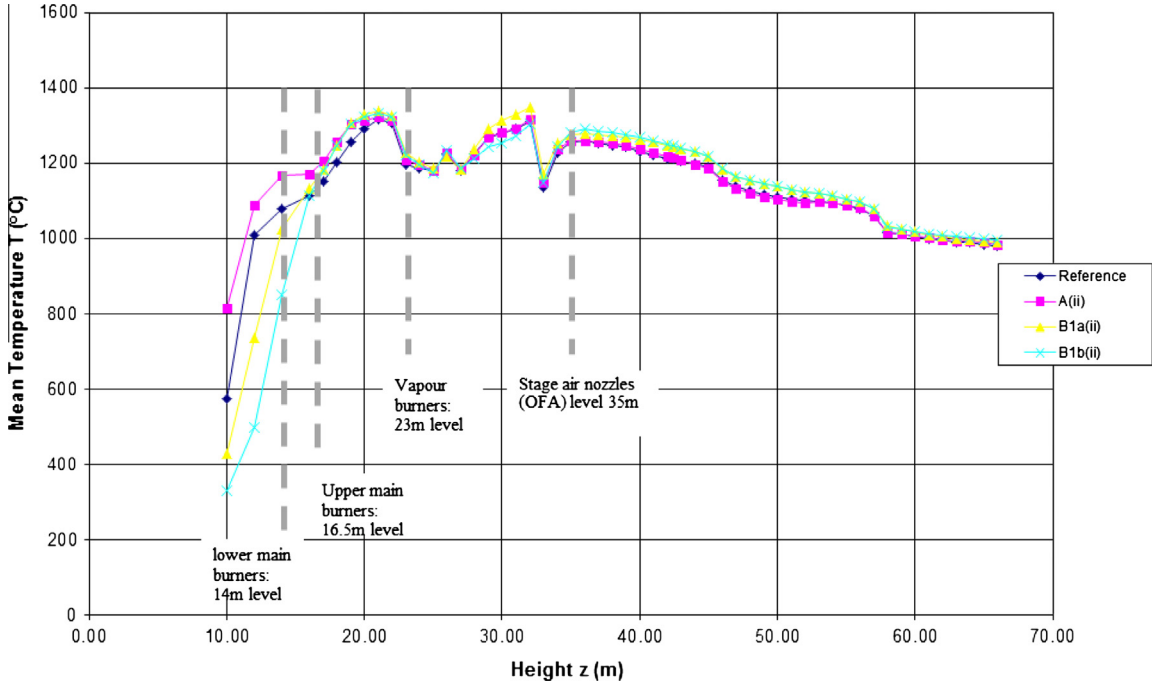

Fig. 13. Distribution of average temperature in height of the boiler for the reference case, A (ii), B1a (ii) and B1b (ii).

70% of the TCI is considered to be covered by own funds of the operator, while the remaining 30% comes from long-term loans, with an interest rate of 7%.

4.2.1.2. Operation and maintenance cost. The cost of Operation and Maintenance (O&M) is divided into fixed and variable. The fixed includes all fixed costs that do not depend on annual production, such as personnel costs, security and cost of planned maintenance work. The variable costs represent the costs arising from the operation of the unit mainly including electricity consumption and consumables. In this work, the O&M cost is considered as 35% of the total investment cost, based on initial cost

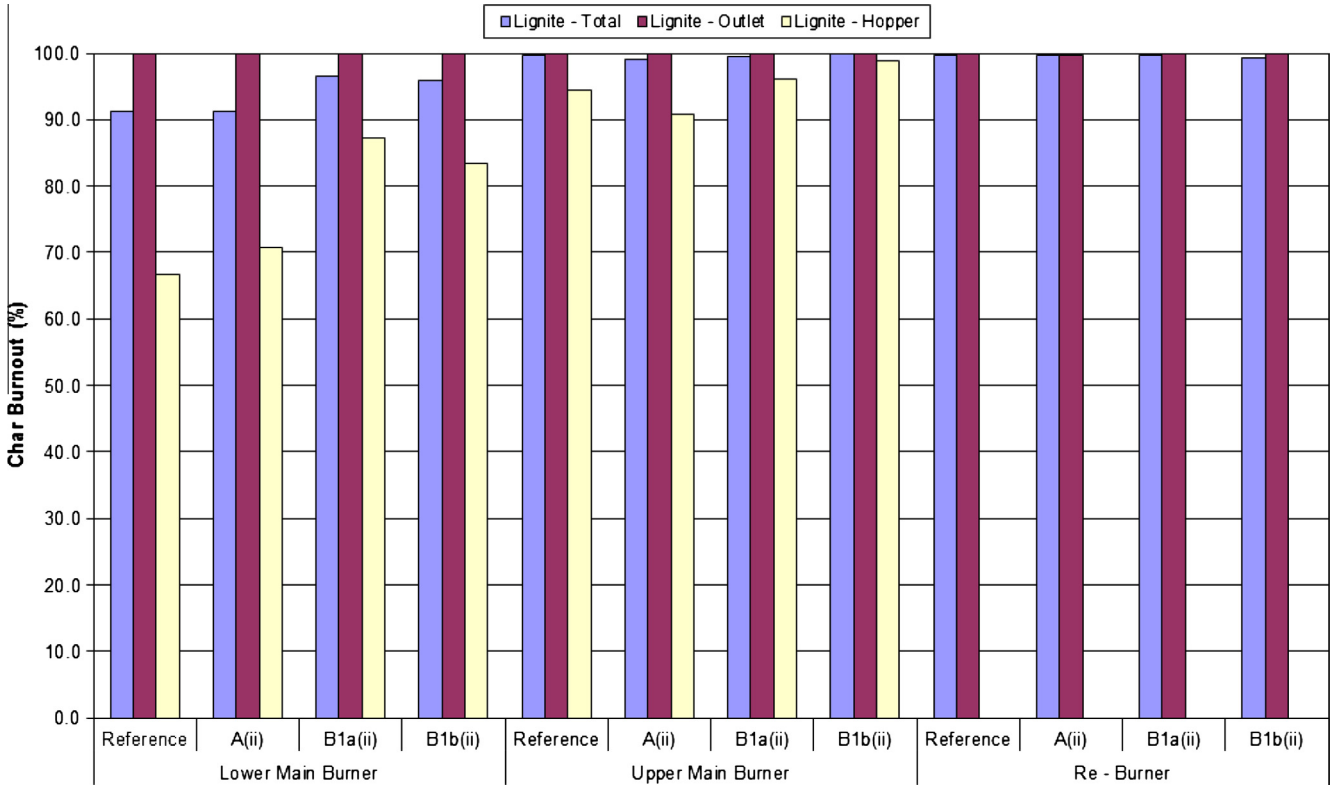

Fig. 14a. Lignite burnout per burner level, overall, at furnace outlet and at ash hopper.

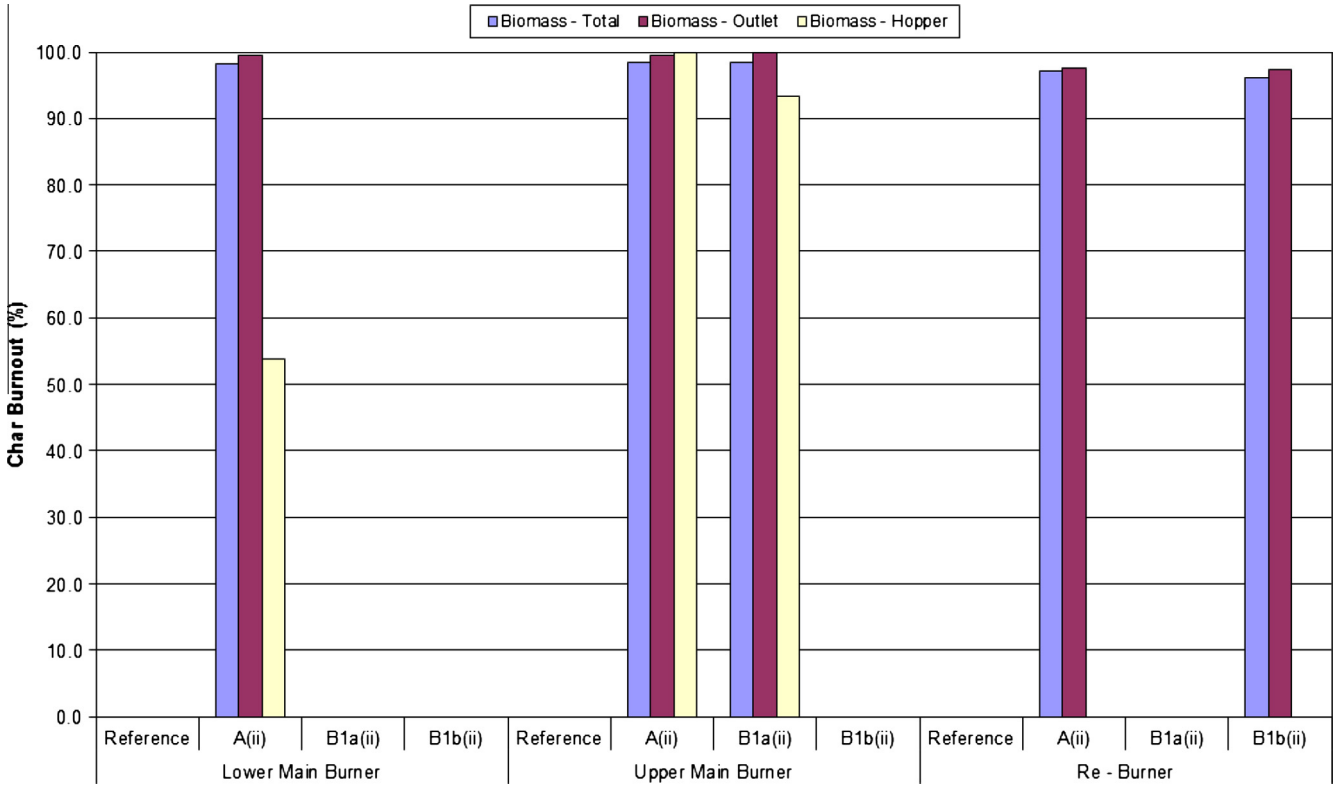

Fig. 14b. Biomass burnout per burner level, overall, at furnace outlet and at ash hopper.

estimates of the electricity consumption, man-hours and spare-part costs for each case.

4.2.1.3. Fuel cost. Co-firing requires significant fuel costs for the purchase of biomass fuel. Currently, there is no established

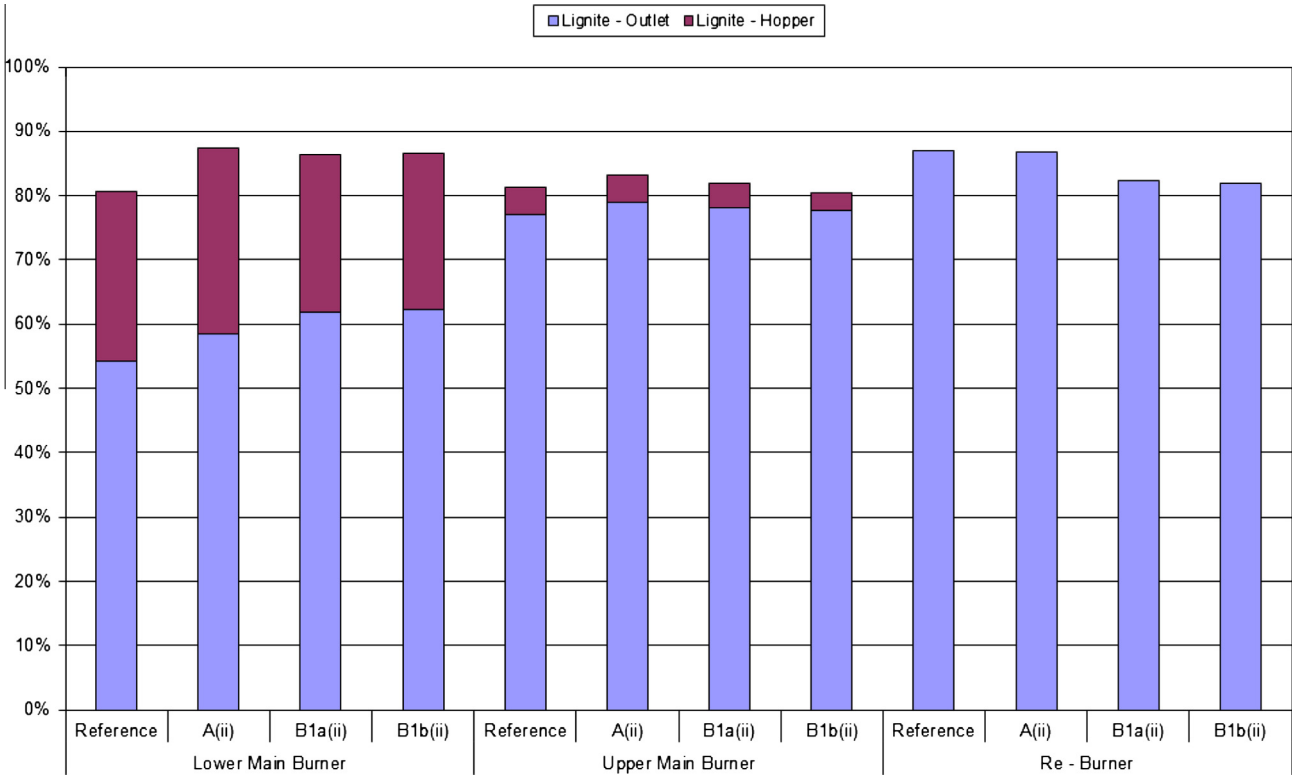

Fig. 15a. Mass percentage of lignite particles leaving the outlet and the ash hopper of the boiler per burner level.

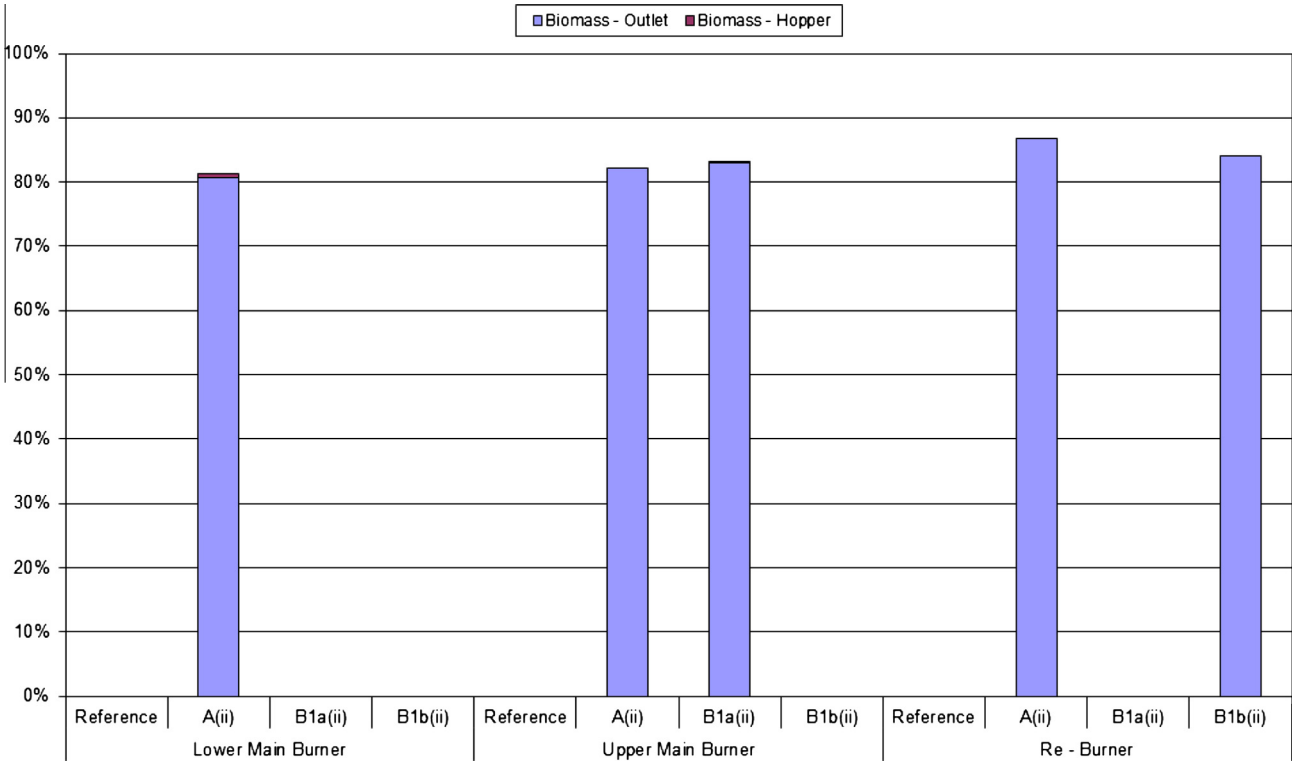

Fig. 15b. Mass percentage of biomass particles leaving the outlet and the ash hopper of the boiler per burner level.

biomass market for co-firing plants in Greece, hence there is great uncertainty in the actual fuel cost; estimations range from 50 €/t to 150 €/t depending among others on the form of the delivered material (pelletized biomass costs more than biomass bales). A

Table 10
Summary of cost categories for Cases A and B.

	Units	Case A	Case B
Total investment cost	€	515,902	1,376,294
Additional fuel cost (biomass cost minus lignite saving)	€/a	17,398,575	6,894,154
O&M costs	€/a	202,161	620,211

Table 11
Additional revenues/savings generated by co-firing.

Additional revenue from biomass feed-in tariff (€)	19,767,600
Savings from CO_2 emissions reduction (€)	9,161,155

Table 12
Parameters used in the economic analysis.

Parameters	Units	Case A	Case B
Thermal substitution	%	10	10
Expected life time	Years	10	10
Development and construction period	Years	1	1
Availability	h/year	7200	7200
Biomass cost	€/t	150	80
Lignite cost	€/t	19	19
Average electricity sale price	€/MW h	55	55
Feed-in tariff for biomass use	€/MW h	150	150
CO_2 emission allowance purchase Cost	€/t CO_2	15	15
Money market rate	%	7	7
Percentage of investment covered by own funds	%	70	70
Percentage of investment covered by loans	%	30	30
Borrowing interest rate	%	7	7
Payback period of loan	Years	10	10
Inflation	%	5	5

Table 13
Financial evaluation criteria for Cases A and B.

	Units	Case A	Case B
Net Present Value (NPV)	€	23,735,926	89,873,631
Internal Rate of Return (IRR)	%	601,071%	998,990%
Payback period	Years	1	1

very high fuel cost can threaten the economic viability of the investment, if the expenditure is much higher than the corresponding revenue.

The price of lignite is also important in the calculation of the fuel cost, since the cost savings achieved by the biomass substitution must be taken into account.

For biomass, an estimated price of 150 €/t is used as a reference for Case A (pellets obtained from the market), while for Case B (biomass bales and shredded material) the cost reference is taken as 80 €/t. The cost of lignite is 2.26 €/GJ or 19 €/t.

The cost breakdown for of the investigated cases is presented at Table 10.

4.2.1.4. Revenues and savings. The expected additional revenues from the application of substitution cases and biomass co-firing are derived from the feed-in tariff of electricity from biomass as set by Law GG 3851/2010 of the Greek legislation. For a biomass capacity higher than 5 MW_e, as is the case for the investigated cases, the feed-in tariff it is set at 150 €/MWh_e.

Thus, the additional revenues from the sale of electricity is resulting from the difference in selling price of electricity from biomass in relation to System Marginal Price (SMP). The SMP is actually determined by the market pool and has significant variations; for the purposes of this study, an indicative constant average value of 55 €/MWh_e is considered.

The economic calculations should also consider the savings for the purchase of CO_2 emissions allowances. This is a variable cost which can be reduced through co-firing since biomass is considered carbon-neutral. After the expiry of the period of the Kyoto Protocol in 2012, the entire amount of CO_2 emissions from lignite combustion will be included in the emissions trading scheme (ETS) and will have to be purchased in the market. It is therefore expected that the operating costs of outdated lignite stations with low efficiencies will be significantly affected. In this context, co-firing is a realistic and reliable option that can bring additional revenue or potential savings of future costs for existing lignite-fired plants. For the emissions trading market, a typical price of 15 €/t CO_2 is considered, which corresponds approximately to the average of recent years. Studies suggest an expected future increase of emissions allowance prices at around 22 €/t CO_2 in the coming years. Nevertheless, the calculations employed the modest price of 15 €/t CO_2 and the effect of variations is studied through parametric risk analysis.

The additional revenues and savings, as calculated, are given in the Table 11 (common to both cases).

Apart from the revenues and expenses which were mentioned above, from which the annual cash flow of the investment is calculated, in order to sum up the Net Cash Flow for the calculation of the Net Present Value, amortization instalments required to repay the loan must be also taken into account. An amount attributable to taxes must also be deducted, assuming a tax rate equal to 25% of income.

The major economic parameters used in the cases considered for the economic analysis are shown in Table 12.

Based on the aforementioned parameters and values, the corresponding values for NPV, IRR and payback period for Cases A and B are presented in Table 13. While both Cases are profitable, Case B is has a higher NPV over Case A as well as the potential for amortization of capital investment in a very short time (1 year). Therefore, Case B is more attractive for the plant operator.

The cumulative cash flow for each of these cases is presented in Fig. 16.

4.2.2. Parametric study and sensitivity analysis to variations in key parameters

As some critical parameters, such as the price of biomass and the cost of purchasing CO_2 allowances, exhibit variations based on market conditions and/or high uncertainty, a sensitivity analysis should be performed in order to evaluate the impact of any

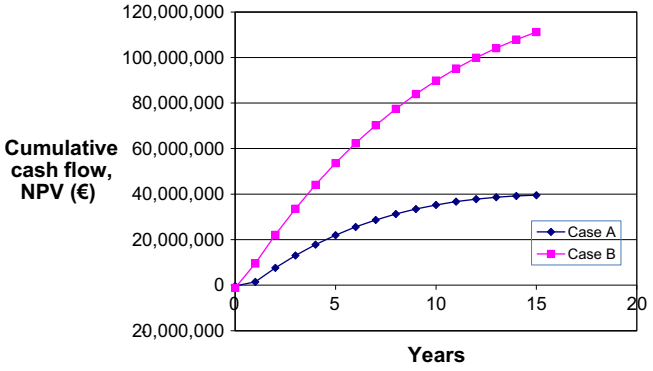

Fig. 16. Cumulative cash flows, expressed as NPV per project year.

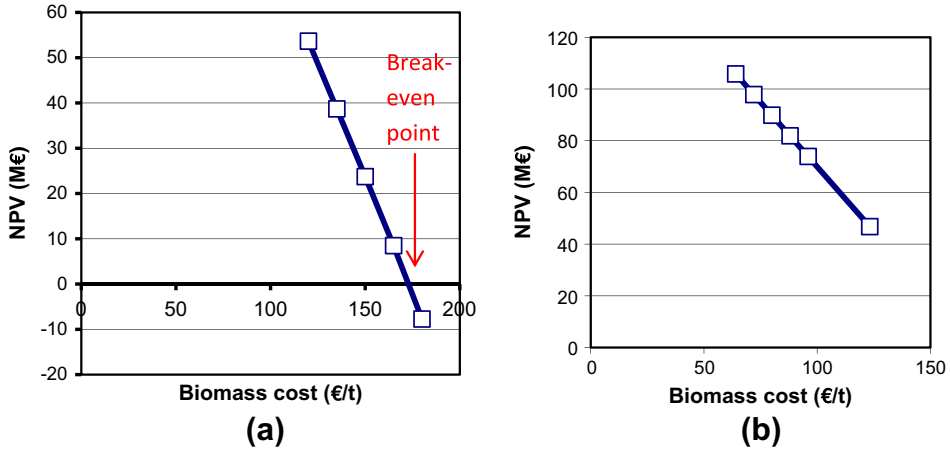

Fig. 17. Sensitivity analysis of NPV to changes in biomass cost for (a) Case A (pellets) and (b) Case B (baled and shredded material).

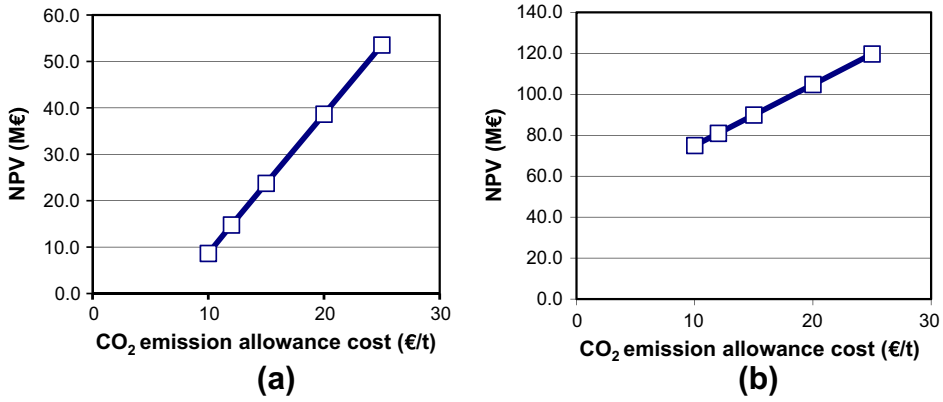

Fig. 18. Sensitivity analysis of NPV to changes in the cost of the purchase of CO_2 emission allowances for (a) Case A and (b) Case B.

changes to their vales as to the co-firing project profitability, as expressed by the NPV. Therefore, the variation in NPV of investment is calculated in relation to the change in the price of biomass (Case A, Fig. 17a and for Case B, Fig. 17b) and the change in the cost of purchasing CO_2 allowances (Case A, Fig. 18a for Case B, Fig. 18b).

From the above it seems that for Case A, a fuel cost over 173 €/t, makes the investment unprofitable. On the other hand, Case B is profitable for all investigated ranges of fuel prices. Moreover, lower costs of CO_2 emission allowances does not seem to threaten the viability of investment, while the expected increase in the coming years yields higher NPVs and makes co-firing even more profitable for both cases.

5. Conclusions

In this paper, the numerical results for a parametric investigation for the operation of a Greek lignite-fired power plant which co-fires biomass at a thermal share of 10% are presented in detail, while a first attempt to compare the financial viability of two biomass handling and feeding scenarios is performed. Overall, the most important operational parameters of the boiler are unaffected by this co-firing concept (low thermal loading), despite slightly increased furnace exit temperatures for some investigates scenarios; the observed increases are not so significant for one to expect intensifying slagging/fouling phenomena related to the lignite particles in comparison with the reference case of operation. The total heat transfer to the furnace wall is likewise unaffected. CFD analysis suggests that a potential benefit of co-firing conditions is the decrease of NO_x emissions up to 10%, due mostly to the lower nitrogen content of the biomass fuel and the respective mechanism for fuel NO_x formation. From this parametric study, it is deduced that in order to achieve satisfactory combustion in the case of biomass and avoid increased unburnt losses, a grinding of the biomass fuel in mean diameters of 0.5–1.0 mm is required; for larger biomass particles (3 mm), a high portion of unburnt char in the ashes is expected. Additionally, large biomass particles result in high temperatures at boiler heights lower than 12 m, which may cause issues to the boiler operation, especially if the substitution percentage is increased to values higher than 10%. In term of injection points, the most efficient case is to inject the biomass particles from the vapour burners, though the upper main burners' level is another possible alternative.

Taking into account possible market prices for fuels and for the equipment required for the co-firing retrofit, an economic evaluation of the different cases suggests that Case B, although more technically complicated and with a higher investment cost, is more profitable. This is mostly due to the lower fuel cost of baled and/or shredded material compared to pellets. The effect of variations of several key parameters such as the price of biomass and the cost of purchasing CO_2 allowances in the viability of the investment also supports this claim.

The results of the economic analysis suggest that an additional investment for dedicated biomass burners is expected to result in profitable projects, while leading to further optimisation of the combustion. Based on the results of this investigation, a suitable level for biomass injection lies at heights higher than the upper main burner level (16.5 m), so as to ensure reduced unburnt losses in the bottom ash and satisfactory burnout of the biomass at the outlet of furnace.

Acknowledgments

The financial grant of the National Cooperation Program 2009 through the ENEP-BIO project (Energetic utilisation of solid and liquid biofuels for the power sector)/Grant No. 09-32-596 and the support of Public Power Corporation S.A. are gratefully acknowledged.

References

[1] Nikolopoulos N, Nikolopoulos A, Karampinis E, Grammelis P, Kakaras E. Numerical investigation of the oxy-fuel combustion in large scale boilers adopting the ECO-Scrub technology. Fuel 2011;90:198–214.
[2] Cho ES, Danon B, de Jong W, Roekaerts D. Behavior of a 300 kWth regenerative multi-burner flameless oxidation furnace. Appl Energy 2011.
[3] Basu P, Butler J, Leon MA. Biomass co-firing options on the emission reduction and electricity generation costs in coal-fired power plants. Renew Energy 2011;36:282–8.
[4] Commission E. Biomass action plan. Official Journal C 49 of 28.02.2005; 2005.
[5] Hansson J, Berndes G, Johnsson F, Kjärstad J. Co-firing biomass with coal for electricity generation—an assessment of the potential in EU27. Energy Policy 2009;37:1444–55.
[6] Dong C, Yang Y, Yang R, Zhang J. Numerical modeling of the gasification based biomass co-firing in a 600 MW pulverized coal boiler. Appl Energy 2010;87:2834–8.
[7] Panoutsou C. Bioenergy in Greece: policies, diffusion framework and stakeholder interactions. Energy Policy 2008;36:3674–85.
[8] Karampinis E, Grammelis P. Current status and future of co-firing in five EU countries: effect of support schemes, sustainability criteria and biomass markets. In: Proceedings of the 19th European biomass conference. Berlin, Germany; 2011.
[9] Skoulou V, Zabaniotou A. Investigation of agricultural and animal wastes in Greece and their allocation to potential application for energy production. Renew Sustain Energy Rev 2007;11:1698–719.
[10] Fernández J, Curt MD, Aguado PL. Industrial applications of *Cynara cardunculus* L. for energy and other uses. Ind Crops Prod 2006;24:222–9.
[11] Grammelis P, Malliopoulou A, Basinas P, Danalatos NG. Cultivation and characterization of *Cynara cardunculus* for solid biofuels production in the Mediterranean region. Int J Mol Sci 2008;9:1241–58.
[12] Karampinis E, Fuller A, Sissot F, Grammelis P, Maier J, Rossi F, et al. Greek lignite/cardoon co-firing: from cultivation to combustion trials. In: Proceedings of ECOS 2011, Novi Sad, Serbia; 2011.
[13] Tillman DA. Biomass cofiring: the technology, the experience, the combustion consequences. Biomass Bioenergy 2000;19:365–84.
[14] Sami M, Annamalai K, Wooldridge M. Co-firing of coal and biomass fuel blends. Prog Energy Combust Sci 2001;27:171–214.
[15] Backreedy RI, Fletcher LM, Jones JM, Ma L, Pourkashanian M, Williams A. Co-firing pulverised coal and biomass: a modeling approach. Proc Combust Inst 2005;30:2955–64.
[16] Gera D, Mathur MP, Freeman MC, Robinson A. Effect of large aspect ratio of biomass particles on carbon burnout in a utility boiler. Energy Fuels 2002;16:1523–32.
[17] Ghenai C, Janajreh I. CFD analysis of the effects of co-firing biomass with coal. Energy Convers Manage 2010;51:1694–701.
[18] Mandø M, Rosendahl L, Yin C, Sørensen H. Pulverized straw combustion in a low-NOx multifuel burner: modeling the transition from coal to straw. Fuel 2010;89:3051–62.
[19] Pallarés J, Gil A, Cortés C, Herce C. Numerical study of co-firing coal and *Cynara cardunculus* in a 350 MWe utility boiler. Fuel Process Technol 2009;90:1207–13.
[20] Yin C, Kær SK, Rosendahl L, Hvid SL. Co-firing straw with coal in a swirl-stabilized dual-feed burner: modelling and experimental validation. Bioresour Technol 2010;101:4169–78.
[21] Yin C, Rosendahl L, Kær SK, Condra TJ. Use of numerical modeling in design for co-firing biomass in wall-fired burners. Chem Eng Sci 2004;59:3281–92.
[22] Asotani T, Yamashita T, Tominaga H, Uesugi Y, Itaya Y, Mori S. Prediction of ignition behavior in a tangentially fired pulverized coal boiler using CFD. Fuel 2008;87:482–90.
[23] Backreedy RI, Jones JM, Ma L, Pourkashanian M, Williams A, Arenillas A, et al. Prediction of unburned carbon and NOx in a tangentially fired power station using single coals and blends. Fuel 2005;84:2196–203.
[24] Choi CR, Kim CN. Numerical investigation on the flow, combustion and NOx emission characteristics in a 500 MWe tangentially fired pulverized-coal boiler. Fuel 2009;88:1720–31.
[25] Díez LI, Cortés C, Pallarés J. Numerical investigation of NOx emissions from a tangentially-fired utility boiler under conventional and overfire air operation. Fuel 2008;87:1259–69.
[26] Modlinski N. Computational modeling of a utility boiler tangentially-fired furnace retrofitted with swirl burners. Fuel Process Technol 2010;91:1601–8.
[27] Vuthaluru HB, Vuthaluru R. Control of ash related problems in a large scale tangentially fired boiler using CFD modelling. Appl Energy 2010;87:1418–26.
[28] Belosevic S, Sijercic M, Oka S, Tucakovic D. Three-dimensional modeling of utility boiler pulverized coal tangentially fired furnace. Int J Heat Mass Transf 2006;49:3371–8.
[29] Belosevic S, Sijercic M, Tucakovic D, Crnomarkovic N. A numerical study of a utility boiler tangentially-fired furnace under different operating conditions. Fuel 2008;87:3331–8.
[30] Tian ZF, Witt PJ, Schwarz MP, Yang W. Numerical modeling of Victorian brown coal combustion in a tangentially fired furnace. Energy Fuels 2010;24:4971–9.
[31] Agraniotis M, Nikolopoulos N, Nikolopoulos A, Grammelis P, Kakaras E. Numerical investigation of Solid Recovered Fuels' co-firing with brown coal in large scale boilers – evaluation of different co-combustion modes. Fuel 2010;89:3693–709.
[32] Karampinis E, Nikolopoulos N, Nikolopoulos A, Grammelis P, Kakaras E. Numerical investigation Greek lignite/cardoon co-firing in a tangentially fired furnace. Appl Energy 2012;97:514–24.
[33] Achim D, Naser J, Morsi Y, Pascoe S. Numerical investigation of full scale coal combustion model of tangentially fired boiler with the effect of mill ducting. Heat Mass Transf 2009;46:1–13.
[34] ANSYS, ANSYS FLUENT 12.0/12.1 Documentation; 2010.
[35] Al-Abbas AH, Naser J, Dodds D. CFD modelling of air-fired and oxy-fuel combustion of lignite in a 100 KW furnace. Fuel 2011;90:1778–95.
[36] Tu J, Yeoh G, Liu C. Computational fluid dynamics — a practical approach. Butterworth-Heinemann: Elsevier Science and Technology; 2007, ISBN: 978-0-7506-8563-4.
[37] Xu M, Azevedo JLT, Carvalho MG. Modelling of the combustion process and NOx emission in a utility boiler. Fuel 2000;79:1611–9.
[38] Xu M, Yuan J, Ding S, Cao H. Simulation of the gas temperature deviation in large-scale tangential coal fired utility boilers. Comput Methods Appl Mech Eng 1998;155:369–80.
[39] Westbrook CK, Dryer FL. Simplified reaction-mechanisms for the oxidation of hydrocarbon fuels in flames. Combust Sci Technol 1981;27:31–43.
[40] Morsi SA, Alexander AJ. An investigation of particle trajectories in two-phase flow systems. J Fluid Mech 1972;55:193–208.
[41] Haider ALO. Drag coefficient and terminal velocity of spherical and nonspherical particles. Powder Technol 1989;58.
[42] Bosoaga A, Panoiu N, Mihaescu L, Backreedy RI, Ma L, Pourkashanian M, et al. The combustion of pulverised low grade lignite. Fuel 2006;85:1591–8.
[43] Vamvuka D, Salpigidou N, Kastanaki E, Sfakiotakis S. Possibility of using paper sludge in co-firing applications. Fuel 2009;88:637–43.
[44] Boyd RK, Kent JH. Three-dimensional furnace computer modeling. In: 21st Symp (Int'l) Combustion; 1986. p. 265–74.
[45] Churchill SW, Bernstein M. A correlation equation for forced convection from gases and liquids to a circular cylinder in cross flow. J Heat Transfer 1977;99:300–6.
[46] Blondeau J, Jeanmart H. Biomass pyrolysis in pulverized-fuel boilers: derivation of apparent kinetic parameters for inclusion in CFD codes. Proc Combust Inst 2011;33:1787–94.
[47] Pyle DL, Zaror CA. Heat transfer and kinetics in the low temperature pyrolysis of solids. Chem Eng Sci 1984;39:147–58.
[48] Yang Y, Sharifi V, Swithenbank J, Ma L, Darvell L, Jones J, et al. Combustion of a single particle of biomass. Energy Fuels 2007;22:306–16.
[49] Bellais M. Modelling of the pyrolysis of large wood particles. KTH Royal Institute of Technology, Stockholm, Sweden; 2007.
[50] Smith IW. The combustion rates of coal chars: a review. In: TC Institute (Ed.), 19 International conference on combustion; 1982. p. 1045–65.
[51] De Soete GG. Overall reaction rates of NO and N2 formation from fuel nitrogen. In: 15th International symposium on combustion, Tokyo, Japan; 1975.
[52] Winter F, Wartha C, Loffler G, Hofbauer H. The NO and N2O formation mechanism during devolatilization and char combustion under fluidized bed conditions. In: 26th International symposium on combustion, Naples, Italy; 1996.
[53] Liu H, Gibbs BM. Modelling of NO and N_2O emissions from biomass-fired circulating fluidized bed combustors. Fuel 2002;81:271–80.
[54] Lockwood FC, Romo-Millares CA. Mathematical modeling of fuel – NO emissions from PF burners. J Inst Energy 1992;65:144–52.
[55] Levy JM, Chen LK, Sarofim AF, Beer JM. NO/char reactions at pulverized coal flame conditions. In: 18th International symposium on combustion, Waterloo, Canada; 1981.
[56] Visona SP, Stanmore BR. Modeling NOx release from a single coal particle II. Formation of NO from char-nitrogen. Combust Flame 1996;106:207–18.
[57] Karampinis E, Sissot F, Grammelis P, Rossi F, Kakaras E. Investigation of wheat straw supply chains for co-firing power plants in Northern Greece. In: 20th European biomass conference and exhibition, Milan; 2012. p. 136–42.
[58] Miltner A, Beckmann G, Friedl A. Preventing the chlorine-induced high temperature corrosion in power boilers without loss of electrical efficiency in steam cycles. Appl Therm Eng 2006;26:2005–11.
[59] Cremers MFG. Technical status of biomass co-firing. IEA Bioenergy Task 32, Deliverable 4; 2009.